STRUCTURAL CONTROL AND HEALTH MONITORING
Struct. Control Health Monit. 2007; **14**:27–61

Time-delayed control design for active control of structures: principles and applications

Firdaus E. Udwadia[1,*,†], Hubertus von Bremen[2] and Phailaung Phohomsiri[1]

[1]*Department of Aerospace and Mechanical Engineering, Civil Engineering, Mathematics and Information and Operations Management, OHE 430K, University of Southern California, Los Angeles, CA 90089-1453, U.S.A.*
[2]*Department of Mathematics and Statistics, California State Polytechnic University, Pomona, California 91768, U.S.A.*

SUMMARY

In this paper we develop the principles of time-delayed control design for the active control of structures in which the presence of large time delays in the control loop may make it difficult for their effects to be easily eliminated and/or compensated. A control design strategy is proposed that is different from what has been generally accepted hereto; it calls for taking advantage of these large, inherent time delays in the control design. The presence of large time delays in the control loop requires that we understand the infinite dimensionality of the system and so we introduce the concept of non-system poles. This is first done within the framework of an SDOF system with time-delayed velocity feedback control. Several new results are presented dealing with stability and performance issues. These results include and extend those available to date. Having developed control design principles with an SDOF system as the underlying basis, these principles are then developed for multi-actuator, multiple time-delay control of MDOF systems. A numerical example of a building structure modeled as an MDOF system that is subjected to strong earthquake ground shaking is presented. The control design based on the underlying principles shows good stability characteristics and effective performance behavior. We demonstrate its application to a structure subjected to strong earthquake ground shaking, thereby showing its usefulness in hazard mitigation.

KEY WORDS: structural dynamics; structural control; time delays; control design; system stability; system performance; multiple actuators; multiple time delays; seismic response; active control

1. INTRODUCTION

Active control of large civil engineering structures requires the capability to sense structural vibrations and deliver appropriate control forces to counteract structural motions. However, time delays inevitably occur in the delivery of the actual control force to a structure because of delays generated in the process of sensing, of computation of the necessary control forces, and

*Correspondence to: Professor Firdaus E. Udwadia, Department of Aerospace and Mechanical Engineering, Mathematics, and Operations Management, 430K Olin Hall, University of Southern California, Los Angeles, CA 90089-1453, U.S.A.
† E-mail: fudwadia@usc.edu

Received 10 February 2004
Revised 2 December 2004
Accepted 18 January 2005

especially because of the limited bandwidth of actuators. Hence the problem of time delays in the active control of structural systems has gained considerable importance and has been investigated by several researchers [1–10]. Most of this work views the presence of time delays in the feedback loop as a detrimental factor and seeks ways to eliminate, nullify, and/or reduce their presumed deleterious effect. Several methods for compensation/nullification have been developed to date, such as, Taylor series [2] and Pade approximations [5], the recursive response method [8], the Smith predictor method [9], state-augmented compensation [8], and predictive response methods. However, such methods can usually be used only when the time delays are small compared with the natural period of the system to be controlled. They generally degrade rapidly from both a stability and a performance perspective when the delays are of the same order of magnitude as the fundamental periods of the structural systems to be controlled. Furthermore, as pointed out elsewhere [2], even with small time delays, Taylor series and polynomial approximations need to be handled with considerable care for they could yield incorrect results.

On the other hand [10–17], time delays can sometimes be used to good advantage in control systems. For example [10,13,16], while non-colocated velocity feedback control is unstable, the addition of a suitable time delay can restore stability. Even in systems modeled by continua [11,12] the proper use of time delays can cause unstable non-colocated control to become stable. The point of view taken in this paper is to accept the fact that time delays—often, large time delays [18,19]—may be present in the feedback control loop when actively controlling large, complex structural systems. We explore the design of structural control systems that utilize the presence of such time delays to some benefit.

We consider first a single-degree-of-freedom system and show that by a proper intentional introduction of a suitable time delay the performance of the system can be brought to about the same level as with direct velocity feedback control. Our presentation differs from past work in the following aspects: (1) we provide a more detailed analysis of time-delayed systems, with emphasis on when the time delays may not necessarily be small; (2) our focus is on the design of time-delayed feedback control to achieve suitable performance and stability when these delays could be of the order of the fundamental period of the system to be controlled.

Past analytical work on time-delayed control has often focused mainly on the use of PID controllers and on determining the maximum time delay that would allow the controlled system to be stable. This is natural because PID controllers are simple to implement and there is ample field experience in their use. Among PID controllers, derivative control is perhaps the most commonly employed, and so in this paper we shall only deal with time-delayed derivative control. Since time delays have been considered to be harmful, the main emphasis so far has been on looking at the effect of small time delays and assessing how large a time delay might lead to instability of the controlled system. In this paper we concentrate on *designing intentional time delays* [16] into the feedback loop to improve stability and performance; except that we work with large time delays. We do not limit ourselves to small time delays, for often a structural system may have large time delays in the control loop [18,19]; and because of this, our analysis in many places needs to be more extensive and detailed. We find that several results believed to be true when dealing only with small time delays need careful restatement and refinement. We find that time-delayed feedback derivative control may often be designed to provide acceptable performance while maintaining good stability characteristics.

In Section 2 of the paper we motivate our study by showing that in the presence of large time delays velocity feedback control can have good performance compared with direct velocity

feedback (with no time delay). Section 3 provides the basic underlying analysis and the development of some principles of time-delayed feedback control in the presence of large (and small) time delays. Both performance and stability aspects of the control design are explored. We begin by considering an SDOF system with time-delayed velocity feedback control. Section 3.1 deals with an analysis of the 'system poles'. These are the poles of the time-delayed system that start (when the feedback gain is zero) at the location of the poles of the uncontrolled system. We show that at a time delay close to the period of the uncontrolled system, the equivalent damping factor of the controlled system can be large. Section 3.2 studies the non-system poles and obtains approximate expressions for their locations. We show that, in general, there are infinitely many non-system poles, and that some of these non-system poles may interact with the system poles as the feedback gain is increased. In Section 3.3 we obtain detailed results on the stability analysis of time-delayed velocity feedback of an SDOF system. These stability results appear to be the most extensive so far obtained. In Section 4 we apply the design principles developed so far to MDOF systems, and provide corroborating numerical results. Section 5 gives the conclusions.

2. PERFORMANCE OF TIME-DELAYED VELOCITY FEEDBACK CONTROL

We begin by considering a single degree-of-freedom (SDOF) system described by the equation

$$\ddot{x} + 2\omega_n\zeta_n\dot{x} + \omega_n^2 x = -g_v\dot{x}(t - T_d) + f(t) \tag{1}$$

where, $\omega_n > 0$ and $0 \leqslant \zeta_n < 1$ are the natural frequency and the damping ratio, respectively, of the uncontrolled system, the velocity feedback is delayed by a time T_d with a gain of g_v, and $f(t)$ is the external excitation. When $g_v > 0$, the negative sign preceding the time-delay term shows that we have negative feedback.

We shall assume in this paper that the uncontrolled system (with $g_v = 0$) is underdamped, as will most likely be the case for structural and mechanical systems. Taking Laplace transforms, the poles of the closed-loop transfer function are given by the zeros of the equation

$$s^2 + 2\omega_n\zeta_n s + \omega_n^2 + g_v s \exp(-sT_d) = 0 \tag{2}$$

From Equation (2) we observe that these zeros occur in complex conjugate pairs. If we imagine an expansion of the exponential term in powers of sT_d, we see that Equation (2) may have an infinite number of zeros and hence the time-delayed system with $g_v \neq 0$ may have an infinite number of poles. In fact, the system is infinite-dimensional. However, for any time delay T_d, when the gain g_v is zero we obtain the zeros of Equation (2) (which are poles of the transfer function) to be the usual complex conjugate 'system poles' of the SDOF oscillator given by $s_{1,\bar{1}} = -\omega_n\zeta_n \pm i\omega_n\sqrt{1-\zeta_n^2}$. When $g_v \neq 0$, these *system poles*, $s_{1,\bar{1}}$ of Equation (2) become functions of the time delay T_d, and the gain g_v; they cannot be found analytically because of the nonlinear nature of the equations, but one can easily obtain them numerically for any given time delay T_d by starting at their known values $s_{1,\bar{1}}$ (just stated) when $g_v = 0$, and finding them in the vicinity of these known values, as g_v progressively increases upwards (or decreases downwards) from zero. We shall call the root loci that begin at the poles of the uncontrolled system (when $g_v = 0$) and that are traced in the complex s-plane as g_v is gradually changed, as the 'root loci of the system poles.'

Figure 1 shows a representative plot of the way in which the system poles, $s_{1,\bar{1}}(T_d, g_v)$, of the controlled system change for different time delays as the gain g_v is increased from 0 to 5 units. All these poles 'begin' at the poles of the uncontrolled system when $g_v = 0$. Since the poles arise in complex conjugate pairs, we show here only the upper complex plane. The uncontrolled system shown in this illustration has a natural period $T_n = 2\pi/\omega_n = 0.804$ s, and a damping factor, $\zeta_n = 1.95\%$.

The value of the dimensionless time delay, $\tau = T_d/T_n$, is indicated adjacent to each curve, and the circles along each curve show the values of the roots of Equation (2) when the velocity feedback gain $g_v = 0$, 1, 2, 3, 4, and 5. We can also think of the time-delayed velocity feedback control as bestowing upon the *given* uncontrolled system (specified by ω_n and ζ_n) an altered set of vibrational characteristics given by an equivalent natural frequency of vibration, $\tilde{\omega}_n(T_d, g_v)$, and an equivalent damping factor, $\tilde{\zeta}_n(T_d, g_v)$. These can be determined from the relations

$$\tilde{\zeta}_n(T_d, g_v) = \frac{\delta}{\sqrt{1+\delta^2}} \qquad \text{and} \qquad \tilde{\omega}_n(T_d, g_v) = \frac{\mathrm{Im}[s_1(T_d, g_v)]}{\sqrt{1-\tilde{\zeta}_n^2}} \tag{3}$$

where

$$\delta = -\frac{\mathrm{Re}[s_1(T_d, g_v)]}{\mathrm{Im}[s_1(T_d, g_v)]} \tag{4}$$

We can then express the system poles, $s_{1,\bar{1}}$, as

$$s_{1,\bar{1}}(T_d, g_v; \omega_n, \zeta_n) = -\tilde{\omega}_n\tilde{\zeta}_n \pm i\tilde{\omega}_n\sqrt{1-\tilde{\zeta}_n^2} \tag{5}$$

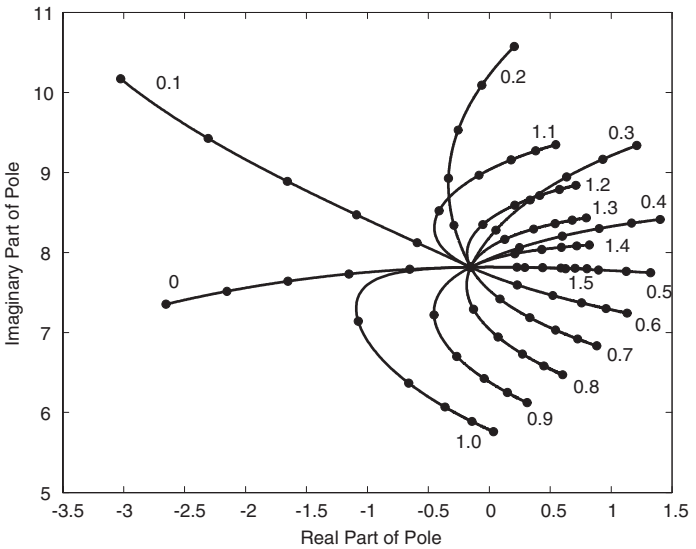

Figure 1. The root locus of the system poles of a time-delayed velocity feedback SDOF system. Each curve corresponds to a fixed value of the dimensionless time delay, $\tau = T_d/T_n$, and emanates from the 'center' at which the feedback gain is zero. Numbers adjacent to each curve give the value of τ for each point along it; the solid circles along each curve indicate, starting from the 'center', successively larger gains, g_v, of 0, 1, 2, 3, 4, and 5.

We note that $\tilde{\omega}_n(T_d, 0) = \omega_n$, and $\tilde{\zeta}_n(T_d, 0) = \zeta_n$. For the range of gains $0 \leqslant g_v \leqslant 5$ explored, there are several important features that Figure 1 shows. (1) For small normalized time delays, τ, of about 0.1 the system is stable. (2) As the time delay increases, the poles have a tendency to bend over into the right half complex plane. The gain and the time delay when the system poles cross over can be easily determined analytically [7]. For example, when the normalized time delay is 0.2, the system pole crosses the imaginary axis when the gain is close to 4. (3) As the normalized time delay gradually increases towards a value of 0.4, the pole crosses over into the right half complex plane at smaller and smaller values of the gain. When $\tau = 0.5$, the pole crosses over at $g_v \simeq 0.3$. (4) However, as the time delay further increases, the curves seem to swing around clockwise (see Figure 1), and the gain at which the pole crosses the imaginary axis again begins to increase. For a normalized time delay, τ, of 0.9, the pole crosses the imaginary axis at a gain of about 3, and when $\tau = 1$, the cross-over occurs at a gain of about 4.7. As we shall see, this increase in the gain when $\tau = 1$ is not entirely fortuitous. (5) For values of $\tau > 1$, the root loci swing around again and seem to wrap around the 'center' even more tightly.

Were we to concentrate our attention solely to the cross-over into the right half complex plane of the root locus we would, as suggested by previous researchers, conclude that time delays are injurious to structural control. Furthermore, were we to restrict ourselves to the investigation of 'small' time delays (say, $\tau = T_d/T_n \leqslant 0.15$) as has been suggested to date [7], we would conclude that time delays lead to instability and that the system could become unstable for even very small gains. Our aim would then be to eliminate such time delays, or ameliorate their effects through compensation/nullification. However, as pointed out above, we notice that for 'large' time delays—time delays of almost the same order as the period of the uncontrolled structural system—the time-delayed control is stable, and in fact it is so over a reasonably wide range of control gains.

It is this behavior for 'large' time delays that we explore in this paper. In fact, in many structural systems significant time delays may arise quite naturally when one considers the delays in sensor and actuator dynamics [18]. Our purpose is to show that through

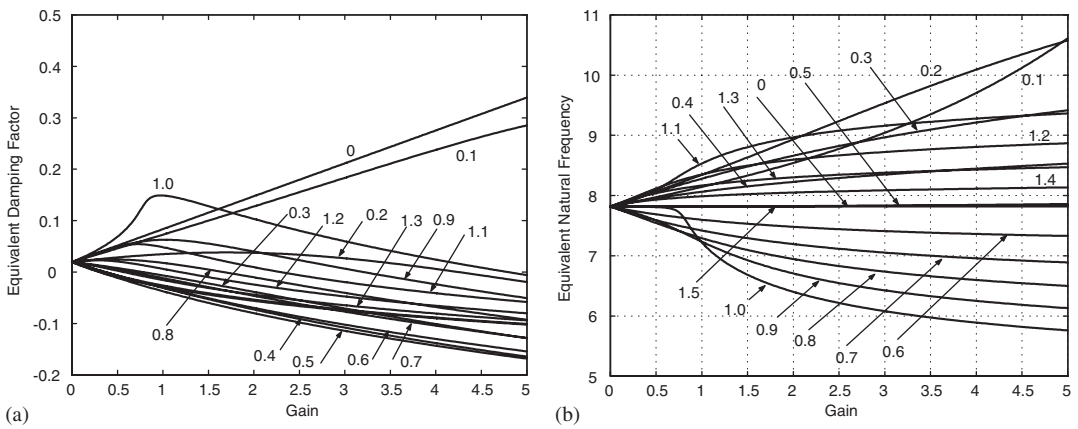

Figure 2. (a) The equivalent damping factor as a function of the gain, g_v. The same data as for Figure 1 is shown. The value of the normalized time delay, $\tau = T_d/T_n$, is shown for each curve. The damping factor for the curve $\tau = 1$ is significantly above that for $\tau = 0$ when the gain is in the vicinity of unity; and (b) equivalent natural frequency corresponding to the system poles. Each curve is for a specific value of τ.

careful design we can take advantage of such time delays and, in fact, by introducing them *intentionally* we can often achieve a control design that, though somewhat inferior, may be almost as good as one where there is no time delay at all. We thus investigate in this paper the possibility of turning what has hereto been thought of as a disadvantage into a potential benefit.

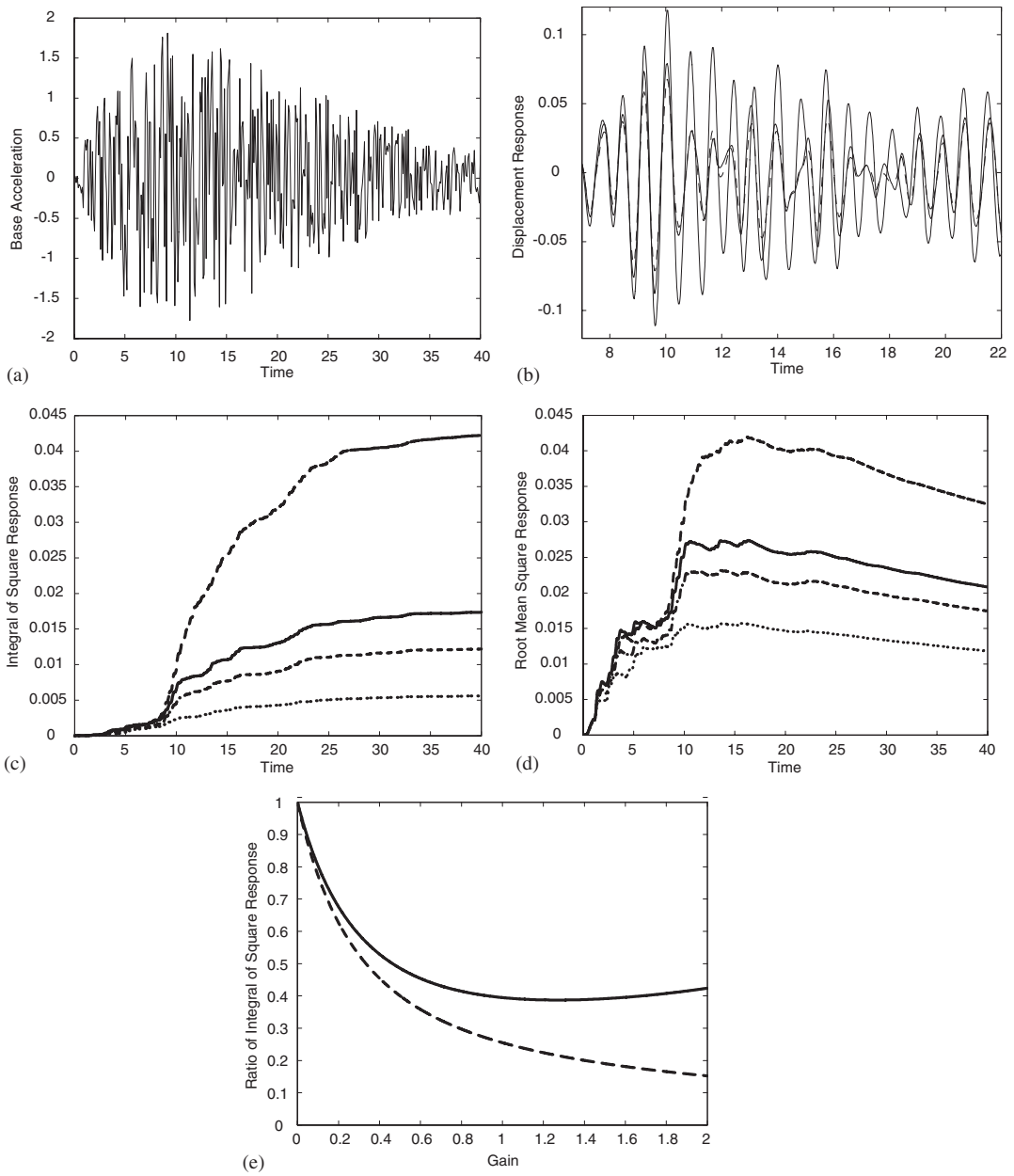

Figure 2(a) shows the variation of the equivalent damping factor $\tilde{\zeta}_n(\tau, g_v)$ for varying values of the feedback gain. Each curve is for a different value of the normalized time delay, τ. When $\tilde{\zeta}_n(\tau, g_v) < 0$, the system is unstable since the pole is in the right half complex plane. The figure shows that for feedback control gains $0 \leqslant g_v \leqslant 1.6$ the time-delayed velocity feedback control with a normalized time delay $\tau = 1$ has a higher value of $\tilde{\zeta}_n$ than that obtained without any time delay. And so one might suspect that the performance of the time-delayed velocity feedback system might be perhaps comparable to that of velocity feedback control with no time delay. Furthermore, for structural systems it is often difficult to generate large control forces and so large gains are normally not practicable. We shall show that, though not the full story, our thinking is indeed along the right lines.

In fact, as shown in the figure, the (equivalent) damping factor for a normalized time delay of unity and a gain of 0.85 is about 14.3%, while that for a similarly controlled system with no time delay is about 7.4%. Hence a choice of an intentional time delay $T_d \simeq T_n$ and a gain of about 0.85 for our velocity feedback control would cause the time-delayed system to have a system pole whose (equivalent) damping factor is about twice the damping factor for velocity feedback control with the same gain and no time delay.

The time delay in the control, however, also affects the equivalent frequency of vibration of the system, $\tilde{\omega}_n(T_d, g_v)$. Its effect on the system poles of the closed loop system is shown in Figure 2(b). We observe that the presence of a time delay could either increase or decrease the equivalent natural frequency, $\tilde{\omega}_n(\tau, g_v)$. We observe that the frequency $\tilde{\omega}_n$ for $\tau = 1$ is less than ω_n and so the system appears 'softer' than one with no time delay. Unless the frequency of the input is known to lie in this reduced frequency range, for relatively broadband inputs this change in the equivalent natural frequency would not greatly affect our control design. The equivalent natural frequency with a time delay $\tau = 1$ and a gain $g_v = 0.85$ drops by 3.8% of its value from that for the uncontrolled system. As noted earlier, for this value of gain and time delay, the improvement obtained in the equivalent damping factor over the damping factor with no time delay is given by

$$\frac{\tilde{\zeta}(\tau = 1, g_v = 0.85)}{\tilde{\zeta}(\tau = 0, g_v = 0.85)} \simeq 1.93.$$

Figure 3. (a) Ground acceleration to which an SDOF structural system with $T_n = 0.804$ and $\zeta_n = 1.95\%$ is subjected; (b) 15 s of the large-amplitude response of the system with direct velocity feedback (dashed line) and time-delayed velocity feedback (solid line) with a time delay $\tau = T_d/T_n = 1$. The gain used in both cases is 0.85. The uncontrolled response of the system is also shown by the solid line which has the large amplitude excursions; (c) integral of the square of the response of the SDOF system with time-delayed velocity feedback (solid line), direct velocity feedback (dash-dot line), and no control (dashed line). The dotted line is for velocity feedback (with no time delay) using the equivalent damping and equivalent frequency of the time-delayed system corresponding to the system poles as given by Equations (3) and (4); (d) root-mean-square response, $\sqrt{1/t \int_0^t x^2(\alpha)\, d\alpha}$, of the response of the SDOF system with time-delayed velocity feedback (solid line), direct velocity feedback (dash-dot line), no control (dashed line), and using equivalent damping factor and frequency of the system poles corresponding to the time-delayed system (dotted line); and (e) ratio of the integral of the square of the response of velocity feedback control with time delay to the integral of the square of the response without control (solid line), and the ratio of the integral of the square of the response of velocity feedback control without time delay to the integral of the square of the response without control (dashed line) as a function of feedback gain.

Figure 3(a) shows a base acceleration, $a(t)$, to which the oscillator is subjected. It is generated by multiplying uniformly distributed random numbers between -1 and 1 with an exponential envelop function to simulate earthquake ground accelerations.

Figure 3(b) shows the response of the two systems during the strong part of the ground motion. The response of the system with time-delayed velocity feedback control using $g_v \simeq 0.85$ and a time delay $T_d = T_n = 0.804$ s is shown, along with the response for velocity feedback using the same gain and no time delay. Figure 3(c) shows the integral of the square of the responses. We see here that though there is some degradation of performance when compared with velocity feedback with no time delay(dash-dot line), the time-delayed control (solid line) is still quite effective in reducing the system's response. For comparison, we also show the results for velocity feedback (with no time delay) of the same SDOF system using the equivalent damping $\tilde{\zeta}(\tau = 1, g_v = 0.85) = 14.3\%$ and the equivalent natural frequency reduced by 3.8% to $\tilde{\omega}_n(\tau = 1, g_v = 0.85) = 7.5127$ rad/s. Figure 3(d) shows the RMS responses with no control (dashed line), time-delayed control (solid line), direct velocity feedback (dash-dot line), and with velocity feedback using the equivalent damping and stiffness values (dotted line). We observe that our time-delayed control performs considerably worse than what might have been predicted using the equivalent frequency and damping determined from the system poles of the time-delayed system. In the next section we shall see why this happens.

Figure 3(e) shows the ratio of the integral of the square of the response (ISR) using velocity feedback control with time delay to the integral of the square of the response without control (solid line) as a function of gain; the ratio of the ISR using velocity feedback control without time delay to the ISR without control as a function of the gain is shown by the dashed line. The values of the ISRs are computed at the end of 40 s of the system's response to ground acceleration shown on Figure 3(a). The results indicate that for any given gain for the range shown, the control of the system with velocity feedback and without time delay is more effective than with time-delayed velocity feedback control. We note, however, that the time-delayed control (see solid line) is nonetheless effective in reducing the response of the system when compared with the response of the uncontrolled system.

3. TIME-DELAYED CONTROL DESIGN PRINCIPLES

3.1. System poles in presence of time delays

In this section we will look at the system poles or the zeros of Equation (2) that start from the zeros of the uncontrolled system ($g_v = 0$). These zeros, as seen in Equation (5), depend on the time delay T_d, on the gain g_v and on the specification of the uncontrolled system ω_n and ζ_n. We shall first show that the system poles can be suitably normalized so that they are made *independent* of ω_n. Then we shall study their behavior and their stability properties.

We begin by dividing Equation (2) by ω_n^2 and putting it in dimensionless form as

$$\tilde{s}^2 + 2\zeta_n \tilde{s} + 1 + \gamma_v \, \tilde{s} \exp(-2\pi\tau\tilde{s}) = 0 \tag{6}$$

where we have denoted

$$\tilde{s} = s/\omega_n, \qquad \tau = \frac{T_d}{T_n} = \frac{\omega_n T_d}{2\pi}, \qquad \text{and} \qquad \gamma_v = \frac{g_v}{\omega_n}$$

All the poles of the closed loop system are now those values of $\tilde{s}$ that satisfy Equation (6).

In particular, for the system poles it is convenient to express them, as before, in terms of the *equivalent* natural frequency of vibration $\tilde{\omega}_n$ and the damping factor $\tilde{\zeta}_n$ of an SDOF system. As stated in Equation (5), these system poles can be expressed as $s_{1,\bar{1}} = -\tilde{\zeta}_n\tilde{\omega}_n \pm i\tilde{\omega}_n\sqrt{1-\tilde{\zeta}_n^2}$, or alternately (since $\tilde{s} = s/\omega_n$) as

$$\tilde{s}_{1,\bar{1}}(\tau, \gamma_v; \zeta_n) = -\tilde{\zeta}_n r \pm ir\sqrt{1-\tilde{\zeta}_n^2} \tag{7}$$

where $r = \tilde{\omega}_n/\omega_n$ is the ratio of the equivalent natural frequency of the time-delayed system to that of the uncontrolled system.

We note from Equation (5) that while $s_{1,\bar{1}}$ is a function of ω_n, $\tilde{s}_{1,\bar{1}}$ by Equation (6) is not; this was the purpose of our normalization. For any given ω_n, the zeros of Equation (2) are then simply obtained by multiplying the corresponding zeros of Equation (6) by ω_n. The appropriate gains g_v are similarly obtained by multiplying the corresponding normalized gains γ_v by ω_n. Furthermore, $\tilde{s}_{1,\bar{1}}(\tau, \gamma_v = 0; \zeta_n) = -\zeta_n \pm i\sqrt{1-\zeta_n^2}$, so that when $\gamma_v = 0$, $r = 1$ and $\tilde{\zeta}_n = \zeta_n$.

Figures 4(a–e) show the system poles, which are the roots of Equation (6) and are given by Equation (7). Since the roots come in complex conjugate pairs, we show only the upper half complex plane. Along the x-axis is plotted $-\tilde{\zeta}_n r$, and along the y-axis is plotted $r\sqrt{1-\tilde{\zeta}_n^2}$ where $r = \tilde{\omega}_n/\omega_n$. The five figures show the roots for different representative values of ζ_n (equal to 0, 0.02, 0.05, 0.07, and 0.1). For a fixed value of τ, as the gain increases, the roots of Equation (6) change. Hence each curve is for a specific value of the dimensionless time delay τ, which is shown along the curve. In each of the five figures all the curves start from $(-\zeta_n, \sqrt{1-\zeta_n^2})$ when the gain $\gamma_v = 0$, representing the uncontrolled system. This point appears as the 'center' from which the curves of constant τ seem to emanate. By successively larger circles along each such curve we have marked the values of the roots for the dimensionless gains $\gamma_v = 0$, 0.1, 0.2, 0.3, 0.4, 0.5, 0.6, and 0.7. Curves for different values of τ varying from zero to 1.5 in steps of 0.1 are shown in each figure. Notice the qualitative change in the behavior of the root loci in the range $1 \leqslant \tau \leqslant 1.1$, which is caused by a bifurcation (see Figure 9).

Each of these figures show that for small gains (that is, in the vicinity of the 'center'), the root loci for $\tau = 0$ and $\tau = 1$ follow the same path. As the gain increases these root loci separate, and the one for $\tau = 1$ bends downwards, thereby causing the equivalent natural frequency of vibration to reduce. However, this root locus moves considerably to the left showing an increase in the equivalent damping factor. It is this property of the root locus of the system poles for $\tau < 1$ that we shall exploit for time-delayed control design. Also, for values of $\tau > 1$, both the equivalent frequency and the equivalent damping increase.

The time-delayed control will certainly lose stability when the root loci cross the imaginary axis. It is important to observe then from Figures 4(a–e) that the stability of the time-delayed system, based on the system poles data presented, depends not only on the value of the time delay used, but also of the feedback gain. One cannot assess the maximum allowable time delay for stability without knowledge of the value of the feedback gain that one wants to use. Furthermore, we shall show that the system poles may *not* dictate the stability of the time-delayed system.

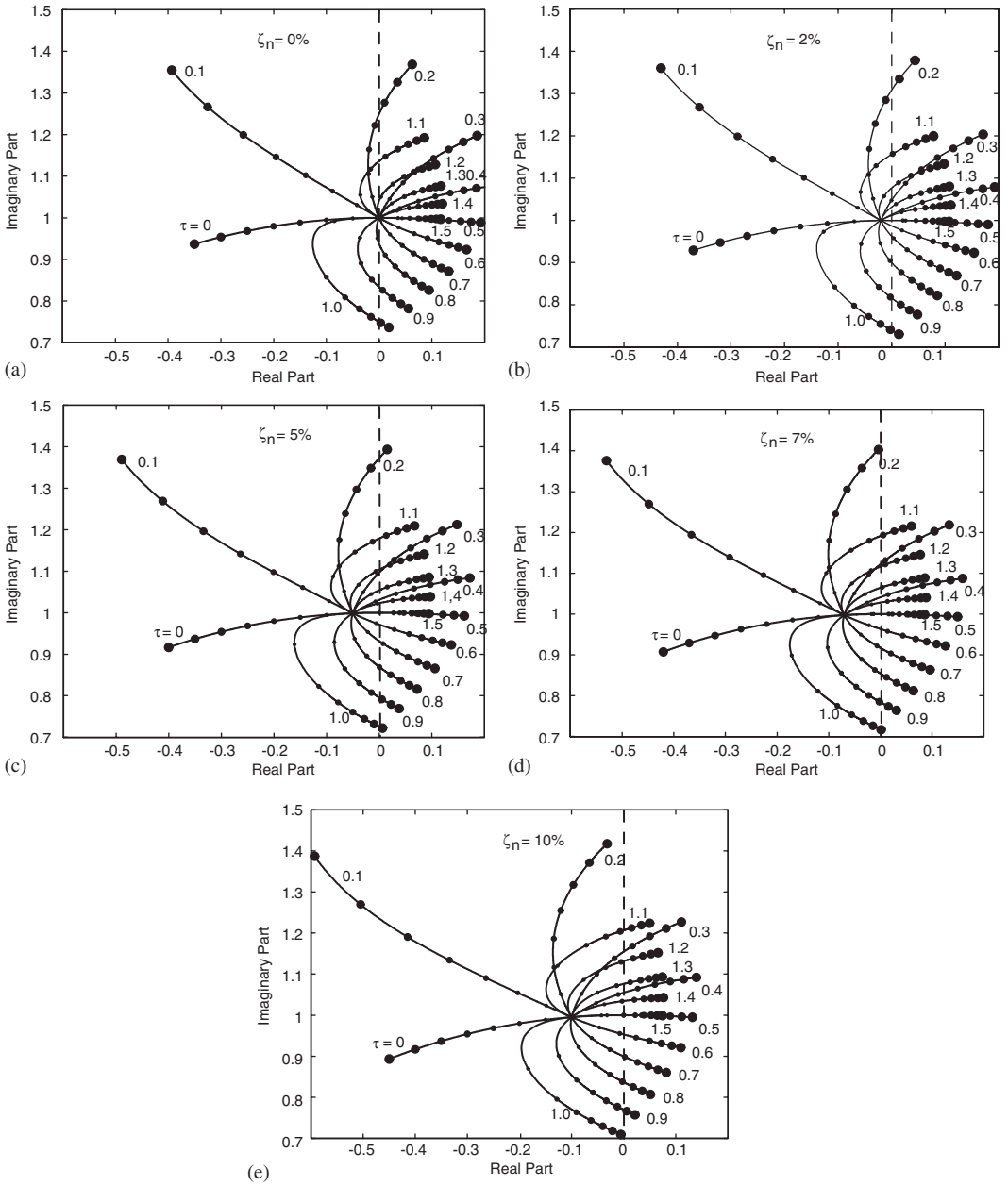

Figure 4. (a–e) The roots (system poles) $\tilde{s}$ of Equation (6) are plotted for five different values of ζ_n. Along the x-axis is plotted $-\tilde{\zeta}_n r$, and along the y-axis is plotted $r\sqrt{1-\tilde{\zeta}_n^2}$ where $r = \tilde{\omega}_n/\omega_n$. Each curve is for a specific value of the time delay τ. Along each curve we plot the values of the dimensionless gain γ_v. Eight different values of the gain are shown along each curve of constant τ, starting from 0 in steps of 0.1 by using successively larger circles. To obtain the poles for any given ω_n, one scales the axes by ω_n.

While Figures 4(a–e) are useful by themselves, we shall try to understand them more deeply by using the following analysis. We note from Equation (6) that

$$\frac{\mathrm{d}\tilde{s}}{\mathrm{d}\gamma_v} = -\frac{\tilde{s}\exp(-2\pi\,\tau\tilde{s})}{2(\tilde{s}+\zeta_n)+\gamma_v\exp(-2\pi\,\tau\tilde{s})[1-2\pi\tau\tilde{s}]} \tag{8}$$

from which it follows that for the pole in the upper half plane

$$\lim_{\gamma_v\to 0}\frac{\mathrm{d}\tilde{s}}{\mathrm{d}\gamma_v} = -\left.\frac{\tilde{s}\exp(-2\pi\,\tau\tilde{s})}{2(\tilde{s}+\zeta_n)]}\right|_{\gamma_v\to 0} = -\frac{1}{2}\left[1+i\frac{\zeta_n}{\sqrt{1-\zeta_n^2}}\right]\exp(2\pi\,\tau\zeta_n)\exp(-2\pi i\tau\sqrt{1-\zeta_n^2}) \tag{9}$$

In the last equality above we have used the relation $\tilde{s}_{1,\bar{1}}(\tau,\gamma_v\to 0;\zeta_n) = -\zeta_n + i\sqrt{1-\zeta_n^2}$. For $\zeta_n \ll 1$ this gives

$$\lim_{\gamma_v\to 0}\frac{\mathrm{d}\tilde{s}}{\mathrm{d}\gamma_v} = -\frac{1}{2}\left[1+i\frac{\zeta_n}{\sqrt{1-\zeta_n^2}}\right]\exp(2\pi\tau\zeta_n)\exp\left[-2\pi i\tau\left\{1-\frac{1}{2}\,\zeta_n^2+\cdots\right\}\right] \tag{10}$$

Hence we get

$$\lim_{\gamma_v\to 0}\frac{\mathrm{d}\tilde{s}}{\mathrm{d}\gamma_v} = -\frac{1}{2}\left[1+i\,\frac{\zeta_n}{\sqrt{1-\zeta_n^2}}\right]\exp(2\pi\tau\zeta_n)\exp(-2\pi i\tau)+O(\tau\zeta_n^2), \qquad \zeta_n \ll 1 \tag{11}$$

which gives

$$\lim_{\gamma_v\to 0}\left.\frac{\mathrm{d}\tilde{s}}{\mathrm{d}\gamma_v}\right|_{\tau=1} = \lim_{\gamma_v\to 0}\left[\frac{\mathrm{d}\ \mathrm{Re}[\tilde{s}]}{\mathrm{d}\gamma_v}+i\,\frac{\mathrm{d}\ \mathrm{Im}[\tilde{s}]}{\mathrm{d}\gamma_v}\right]\Bigg|_{\tau=1} = -\frac{1}{2}\left[1+i\,\frac{\zeta_n}{\sqrt{1-\zeta_n^2}}\right]\exp(2\pi\zeta_n)+O(\zeta_n^2) \tag{12}$$

From Equation (12) we see that the rates of change of both $\mathrm{Re}(\tilde{s})$ and of $\mathrm{Im}(\tilde{s})$ along the curve $\tau = 1$ are both negative as $\gamma_v \to 0$, for $\zeta_n \ll 1$. Also, the slope of the root locus as $\gamma_v \to 0$ equals ζ_n (to order ζ_n^2) along the root locus for $\tau = 1$, which is the same as that for the root locus along the curve $\tau = 0$ as seen from Equation (11). What we have shown is that for small values of γ_v and ζ_n, the root loci for velocity feedback with no time delay and for velocity feedback with a time delay of $\tau = 1$ start from the 'center' and remain close to one another. Figures 4(a–e) corroborate this result.

When $\tau = 1/2$, we have

$$\lim_{\gamma_v\to 0}\left.\frac{\mathrm{d}\tilde{s}}{\mathrm{d}\gamma_v}\right|_{\tau=1/2} = \lim_{\gamma_v\to 0}\left[\frac{\mathrm{d}\ \mathrm{Re}[\tilde{s}]}{\mathrm{d}\gamma_v}+i\,\frac{\mathrm{d}\ \mathrm{Im}[\tilde{s}]}{\mathrm{d}\gamma_v}\right]\Bigg|_{\tau=1/2} = \frac{1}{2}\left[1+i\,\frac{\zeta_n}{\sqrt{1-\zeta_n^2}}\right]\exp(\pi\zeta_n)+O(\zeta_n^2) \tag{13}$$

showing that the rates of change of both $\mathrm{Re}(\tilde{s})$ and $\mathrm{Im}(\tilde{s})$ are positive along the curve $\tau = 1/2$, as $\gamma_v \to 0$ for $\zeta_n \ll 1$. However, the slope of the root locus along this curve as $\gamma_v \to 0$, and $\zeta_n \ll 1$, is, as before, equal to ζ_n. These results are exhibited in the plots of Figures 4(a–e). Clearly then one can conjecture that the time-delayed control may be effective for *negative* gains (*positive* feedback) for then the rates of change of $\mathrm{Re}(\tilde{s})$ and $\mathrm{Im}(\tilde{s})$ will both be negative along the curve $\tau = 1/2$, as $\gamma_v \to 0$ for $\zeta_n \ll 1$. We shall show in the next section that this indeed is true.

Lastly, from Equation (9), we see that the slope of the root locus at the 'center' is zero whenever

$$\tau = \tau_n^* = \frac{1}{2\pi\sqrt{1-\zeta_n^2}} \tan^{-1}\left(\frac{\zeta_n}{\sqrt{1-\zeta_n^2}}\right) + \frac{n}{2\sqrt{1-\zeta_n^2}}, \qquad n = 0, 1, 2, 3, \ldots \tag{14}$$

The root locus moves leftwards when n is even and rightwards when n is odd. For $\zeta_n \ll 1$, this occurs, from Equation (14), when $\tau \simeq n/2$, $n = 0, 1, 2, 3, \ldots$. Furthermore, the absolute value of the slope becomes infinity (that is, the root locus takes off vertically from the center as the gain γ_v is increased infinitesimally from zero) when

$$\tau = \frac{1}{2\pi\sqrt{1-\zeta_n^2}} \tan^{-1}\left(-\frac{\sqrt{1-\zeta_n^2}}{\zeta_n}\right) + \frac{n}{2\sqrt{1-\zeta_n^2}}, \qquad n = 0, 1, 2, 3, \ldots \tag{15}$$

For $\zeta_n \ll 1$, from Equation (15), this occurs when $\tau \simeq \frac{(2n+1)}{4}$, $n = 0, 1, 2, \ldots$. For a system with $\zeta_n = 0$, if one progressively increases the time delay starting from $\tau = 0$, at a time delay of $\tau = 1/4$ the root locus will take off from the center (whose abscissa in the $\tilde{s}$-plane is 0, since $\zeta_n = 0$) vertically. The maximum time delay for stability, in the sense described above, would then be $\tau = 1/4$. However, for *any* value of ζ_n close to zero *but positive*, the maximum time delay for stability, again were we progressively to increase the time delay starting from $\tau = 0$, would have to first occur when Equation (14) is satisfied with the pole moving rightward, and this would be around $\tau = 1/2$. Since the slope of the root locus would be zero when Equation (14) is satisfied, and since the root locus would have to travel approximately a horizontal distance ζ_n, the maximum gain for stability for $\tau = 1/2$ can be approximated using Equation (11) as

$$\gamma_v\big|_{max} = -\left.\frac{2\zeta_n \exp(-2\pi\,\tau\zeta_n)}{\cos(2\pi\tau) + \zeta_n \sin(2\pi\tau)}\right|_{\tau=1/2} \simeq 2\zeta_n \qquad \text{when } \tau\zeta_n \ll 1 \tag{16}$$

For values of $n > 1$ in Equation (14), this approximate way of determining the maximum gain for stability loses its validity because the root loci wind themselves more tightly around the center as n increases. Equation (16) then says that for almost all SDOF systems met with in real-life—systems for which $0 < \zeta_n \ll 1$—were we to progressively increase the time delay τ from zero while using time-delayed negative velocity feedback, we would find: (1) that the smallest gain beyond which the system becomes unstable is $2\zeta_n$, and (2) that this *first* happens when the time delay is approximately half the natural period of the uncontrolled system. Thus the smallest gain that causes such a system to become unstable first (when starting from zero time delay) occurs at $\tau \approx 1/2$ and *not* at $\tau \approx 1/4$. For a computational verification of this see the curve for $\tau = 1/2$ in Figure 2(a). We shall show in the next sub-section that an even more general relation than Equation (16) (and the previous statement) can be obtained, as shown in Figure 11.

It is interesting that for $0.01 \leqslant \zeta_n \leqslant 0.07$ the three sets of curves (see Figures 4b–d), when displaced so that their centers coincide, appear to fall approximately on top of each other for purposes of control design. Thus upon such a displacement of each set of curves (each set is drawn corresponding to a fixed value of ζ_n) it appears that nearly the same curves are traced out for each value of τ; however, along each of these curves of constant τ, the values of γ_v are not the same.

Figure 5 shows the equivalent damping factor, $\tilde{\zeta}_n$, for $\zeta_n = 0.02$ and 0.05 as a function of the gain with time-delayed negative velocity feedback. The figure shows the sharp rise in the equivalent damping factor around $\tau = 1$. Note that there is a range of gains for $\tau = 1$ over which the equivalent damping of the time-delayed system, considering only the system poles, is higher than that of the system with no time delay and direct velocity feedback. In Figure 6 we show similar plots for the normalized equivalent natural frequency $r = \tilde{\omega}_n/\omega_n$.

It appears advantageous, from a design standpoint to use intentional time delays of $\tau \simeq 1$, and a gain at which the $\tilde{\zeta}_n$ is close to its peak. Around where this peak occurs, the equivalent natural frequency is also altered. As shown in Figure 6, depending on the value of τ it could be increased or decreased when compared with the natural frequency of the uncontrolled system.

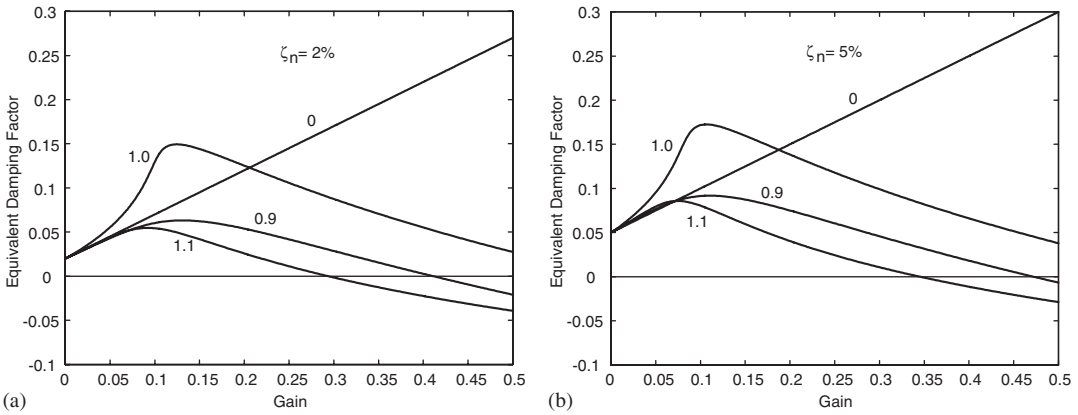

Figure 5. Equivalent damping $\tilde{\zeta}_n$ as a function of the gain γ_v for system poles. Each curve is for a different time delay which is stated next to it. We show curves only for τ =0, 0.9, 1.0, and 1.1.

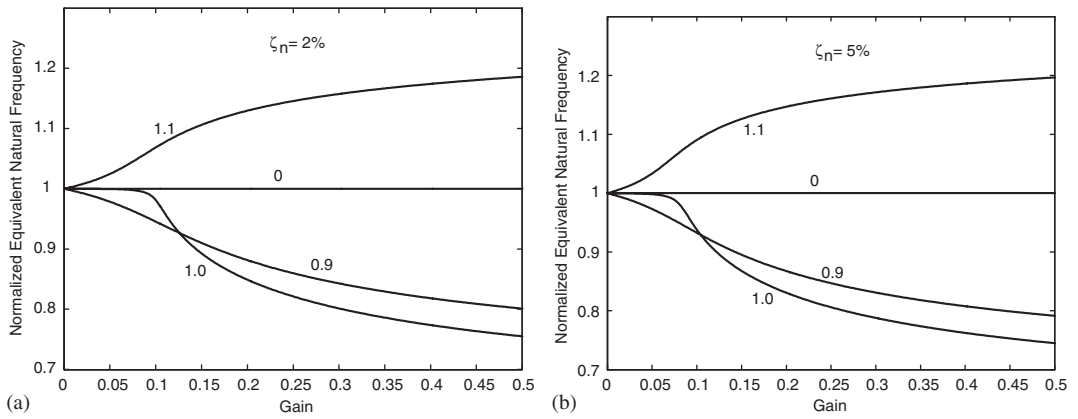

Figure 6. Normalized equivalent natural frequency r as a function of the gain γ_v for system poles. Each curve is for a different time delay which is stated next to it.

Figures 5 and 6 can be used for design purposes. They show the equivalent damping ratio and the equivalent frequency as a function of the time delay and the gain. However, while curves such as those shown in Figures 5 and 6 are very useful in the design of time-delayed velocity feedback control, when using large, intentional time delays, we shall see in the next section that they must be used with considerable care for the system's behavior may not be fully captured by its 'system poles.'

3.2. Non-system poles in presence of time delays

We have seen in Figures 3(c) and 3(d) that were we to consider the time-delayed system as an equivalent SDOF system with an equivalent damping factor $\tilde{\zeta}_n$ and equivalent natural frequency $\tilde{\omega}_n$, the response of this system (for the parameters chosen) is nowhere near the response of the actual time-delayed system to the base acceleration shown in Figure 3(a). The degradation of the response of the time-delayed system from what one might expect when using the equivalent damping and natural frequency is caused by the presence of non-system poles, poles that stream in from $-\infty$ in the complex s (or $\tilde{s}$) plane. We now study these non-system poles. We shall primarily concern ourselves here with negative feedback.

We begin again with Equation (6) and write $\tilde{s} = R\exp\{i(\pi - \varphi)\} = -R\exp(-i\varphi)$, where R is a real, positive number, the angle φ being measured in the *clockwise* direction from the negative real axis. Equation (6) whose zeros give the poles of the time-delayed velocity feedback system, now becomes

$$\frac{R^2 e^{-2i\varphi} - 2\zeta_n R e^{-i\varphi} + 1}{R\exp(2\pi\tau R\cos\varphi)} = \gamma_v e^{-i\varphi}\exp(-2\pi i\tau R\sin\varphi) \tag{17}$$

3.2.1. Behavior of Non-system Poles as $\gamma_v \to 0$. We shall show that when there is a time delay, the only roots of Equation (17) as $\gamma_v \to 0$ are either the system poles or poles at ∞ such that $R \to \infty$. Furthermore, as $\gamma_v \to 0$, there can be no poles either on the imaginary axis (unless $\zeta_n = 0$) or in the right half complex $\tilde{s}$-plane. Roughly speaking, the non-system poles start from $R = \infty$ in the left half complex plane when the gain $\gamma_v = 0$, and gradually move rightwards as the gain is increased.

1. If $\varphi = 0$, and $\tau > 0$, Equation (17) gives

$$\frac{R^2 - 2\zeta_n R + 1}{R\exp(2\pi\tau R)} = \gamma_v \tag{18}$$

and taking the limit as $\gamma_v \to 0^+$, (the superscript indicates that γ_v goes to zero over positive values) we see from Equation (18) that either $R^2 - 2\zeta_n R + 1 = 0$, or R must tend to ∞ so that the exponential term in the denominator dominates and causes the left-hand side to go to zero. But $R^2 - 2\zeta_n R + 1 = 0$ causes R to be complex, which cannot be since R must be real. Hence, as $\gamma_v \to 0^+$, there is a pole of the time-delayed system for $\varphi = 0$, and $R \to \infty$. In other words, there is a pole for time-delayed negative velocity feedback that lies on the negative real axis (in the $\tilde{s}$-plane) and tends to $-\infty$ as $\gamma_v \to 0$.

We also see from Equation (18) that for $\tau = 0$, there can be no pole along the negative real axis for negative velocity feedback for values of the gain $\gamma_v < 2(1 - \zeta_n)$. For time-delayed positive feedback, no poles exist along the negative real axis $\tilde{s}$-plane for $\tau \geqslant 0$ and $0 \leqslant \zeta_n < 1$, no matter what the magnitude of the gain.

2. If $0<|\varphi|<\pi/2$ and $\tau\geqslant 0$, from Equation (17) we get

$$\left|\frac{R^2\cos 2\varphi - 2\zeta_n R\cos\varphi + 1 \pm i(2\zeta_n R\sin\varphi - R^2\sin 2\varphi)}{R\exp(2\pi\tau R\cos\varphi)}\right| = |\gamma_v|$$

Thus, as $\gamma_v \to 0^{+,-}$, we require that, if R is finite, the imaginary part and real part of the numerator on the left-hand side, each, equal zero. The imaginary part requires that $\cos(\varphi) = \zeta_n/R$. Using this relation, in $R^2\cos 2\varphi - 2\zeta_n R\cos\varphi + 1 = 0$, we get $R = 1$, which is the location of the system pole. Thus as $\gamma_v \to 0^{+,-}$, the non-system poles should be at $R \to \infty$.

3. If $\varphi = \pm\pi$, then $\tilde{s} = R$ with R real and positive, and Equation (17) becomes

$$\left\{R + 2\zeta_n + \frac{1}{R}\right\} = -\gamma_v\exp(-2\pi\tau R) \tag{19}$$

But Equation (19) is impossible to satisfy for any real, positive value of R for *any* non-negative value of γ_v. Hence there cannot be any poles along the positive real axis in the $\tilde{s}$-plane for any value of the time delay for negative velocity feedback. For positive velocity feedback, no poles exist on the real positive axis in the complex $\tilde{s}$-plane for $\gamma_v > -2(1+\zeta_n)$ when $\tau\geqslant 0$.

4. If $\varphi = \pm\pi/2$, then $\tilde{s} = R\exp\{i(\pi-\varphi)\} = \pm iR$ and Equation (17) then yields

$$\left|\frac{1 - R^2 \pm 2i\zeta_n R}{R}\right| = |\gamma_v| \tag{20}$$

Hence for $\zeta_n \neq 0$, as $\gamma_v \to 0^{+,-}$, there cannot be a pole on the imaginary axis; and for $\zeta_n = 0$, the only pole on the imaginary axis as $\gamma_v \to 0^{+,-}$ must have an ordinate of ± 1 which, of course, is the system pole! Hence there are no non-system poles along the imaginary axis as $\gamma_v \to 0$.

5. If $\varphi = \pm(\psi + \pi/2)$, for $0<\psi<\pi/2$, then Equation (17) gives

$$\exp(2\pi\tau R\sin\psi)\left|-Re^{\mp 2i\psi} \pm 2i\zeta_n e^{\mp i\psi} + \frac{1}{R}\right| = |\gamma_v| \tag{21}$$

As $\gamma_v \to 0^{+,-}$, the left-hand side of Equation (21) must also tend to zero. Hence we must have

$$\cos\psi(R\sin\psi + \zeta_n) = 0 \tag{22}$$

which is impossible for $0<\psi<\pi/2$, since $\zeta_n\geqslant 0$, and $R>0$. Hence, there are no poles (system or non-system) that lie in the right half complex plane as $\gamma_v \to 0^+$. There are no non-system poles on the imaginary axis as $\gamma_v \to 0^+$. When $\zeta_n = 0$, only the system poles lie on the imaginary axis as $\gamma_v \to 0^+$. A more general analysis than that of this sub-section is available [16].

3.2.2. Location of non-system poles and their interaction with system poles. In this sub-section we shall deal only with time-delayed *negative* velocity feedback. We first consider the rate at which the poles which are at $R \to \infty$ in the left half complex plane when $\gamma_v \to 0$ move as we gradually increase the negative feedback gain, γ_v. Taking the derivative of Equation (6) with respect to γ_v, we get, as we did in Equation (8)

$$\tilde{s}' = \frac{d\tilde{s}}{d\gamma_v} = \frac{-\tilde{s}\exp(-2\pi\tau\tilde{s})}{2(\tilde{s}+\zeta_n) + \gamma_v\exp(-2\pi\tau\tilde{s})(1-2\pi\tau\tilde{s})} \tag{23}$$

Using Equation (6) to replace the exponential terms in Equation (23), we get

$$\tilde{s}' = \frac{\tilde{s}}{\gamma_v}\left[\frac{1}{2\pi\tau\tilde{s} + 1 - \dfrac{2(\zeta_n\tilde{s}+1)}{\tilde{s}^2 + 2\tilde{s}\zeta_n + 1}}\right] \tag{24}$$

Setting $\tilde{s} = -R\exp(-i\varphi)$, as before, and considering the above expression for values of $R \gg 1$, we can approximate it as

$$\begin{aligned}\tilde{s}' &\simeq \frac{\tilde{s}}{\gamma_v}\left[\frac{1}{2\pi\tau\tilde{s} + 1 + O\left(\dfrac{\zeta_n}{R}\right)}\right] \\ &= \frac{1}{2\pi\tau\gamma_v}\left[\frac{1 - \dfrac{\cos\varphi}{2\pi\tau R}}{1 - \dfrac{\cos\varphi}{\pi\tau R} + O\left(\dfrac{1}{R^2}\right)}\right] + \frac{i}{\gamma_v}\left[\frac{\sin\varphi}{4\pi^2\tau^2 R\left[1 + O\left(\dfrac{1}{\tau R}\right)\right]}\right]\end{aligned} \tag{25}$$

Hence, we have

$$\tilde{s}' \simeq \frac{1}{2\pi\gamma_v\tau} + O\left(\frac{1}{\gamma_v\tau^2 R}\right) + \frac{i}{4\pi^2\gamma_v\tau^2 R}\sin\varphi \approx \frac{1}{2\pi\gamma_v\tau} + iO\left(\frac{1}{\gamma_v\tau^2 R}\right) \tag{26}$$

This expression tells us that for $R \gg 1$ the rate of change of the real part of the non-system poles goes inversely as the product $\gamma_v\tau$. The rate of change of the real part of the pole reduces as the gain is increased and/or the time delay is increased. The rate of change of the imaginary part of the pole is much less than that of the real part, and is of $O(1/\gamma_v\tau^2 R)$. As the first term on the right in Equation (26) shows, for very small gains, the real part of the pole moves rapidly rightwards into the complex $\tilde{s}$-plane, the imaginary part changes little.

The picture that emerges then is as follows. The non-system poles emerge from the left half complex plane and 'stream' rightwards as the gain is increased; they move almost horizontally across the complex plane as long as the product $\gamma_v\tau^2 R \gg 1$.

Figures 7(a) and 7(b) show the non-system poles for a time delay $\tau = 1$ and for damping factors $\zeta_n = 0.02$, and $\zeta_n = 0.05$. The root loci of these poles have been plotted for values of the gain ranging from 0.0001 to 0.7. Circles along each root locus show the locations of the poles at γ_v =0.01, 0.03, 0.05, 0.07, 0.09, 0.1, 0.2, 0.3, 0.4, 0.5, 0.6 and 0.7. The leftmost point on each locus is the location of the pole when γ_v =0.0001. As seen, the poles stream in as the gain is increased, moving rightwards. The solid line shows the system pole. The figures show that the system pole can interact with the non-system poles, often exhibiting interesting behavior—such as bifurcations—that can affect the stability of the time-delayed system [16].

In Figure 7(a) we see this interaction occurring for the lowest two non-system root loci as the gain increases. The non-system pole with an ordinate of about 1.06 is 'deflected' upwards when it approaches the system pole as shown in the Figure 7(a). The presence of this non-system pole in the vicinity of the system pole causes the non-system pole to accelerate rightwards; it crosses the imaginary axis at a gain of about 0.4737. Careful analysis of the interaction of the system pole and this non-system pole shows that in the vicinity of $\tau = \tau_b \simeq 1.015345$ a bifurcation occurs when the non-system pole 'collides' with the system pole, which then loses its virgin

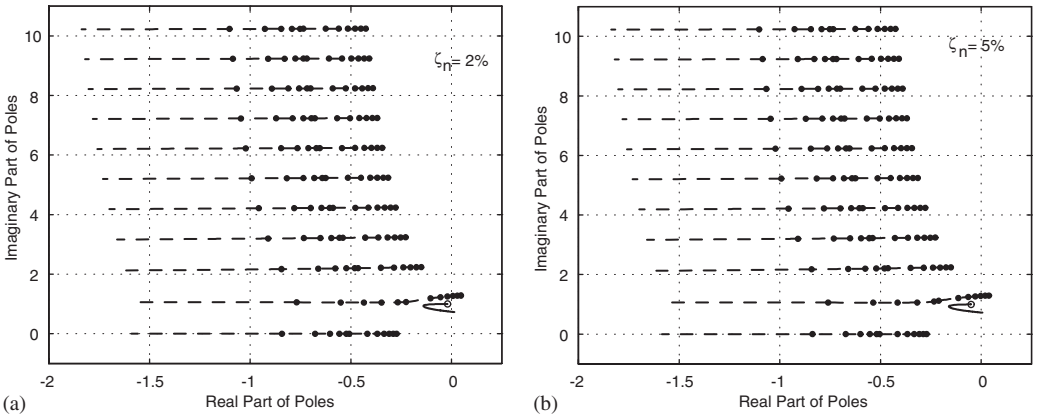

Figure 7. The root loci of poles for time-delayed negative velocity feedback with $\tau = 1$: (a) $\zeta_n = 2\%$; and (b) for $\zeta_n = 5\%$. The solid line shows the root locus of the 'system' pole as the gain changes from 0 to 0.7; the open circle is the location of the pole for the uncontrolled system. The 'non-system poles' root loci (dashed lines) are shown for values of the gain ranging from 0.0001 to 0.7. The solid circles along each root locus show the locations of the non-system poles for γ_v =0.01, 0.03, 0.05, 0.07, 0.09, 0.1, 0.2, 0.3, 0.4, 0.5, 0.6 and 0.7.

identity (see discussion on Figure 9). For values of $\tau > \tau_b$ the non-system pole gets 'deflected' downwards.

Comparing Figures 4(b) and 7(a), each of which correspond to $\zeta_n = 0.02$, we see that the stability of the time delayed system when $\tau = 1$ is thus controlled by this non-system pole. While Figure 4(b) might seem to show that the system remains stable for gains up to $\gamma_v \simeq 0.613$, we must recall that this figure shows only the system poles; the non-system poles that starts at $-\infty$ 'stream in' as the gain is gradually increased from zero; in fact the one that starts with an ordinate of about 1.06 (see Figure 7a) outpaces the system pole as the gain is increased, and crosses the imaginary axis at a gain of $\gamma_v \simeq 0.473$. Thus, it is this non-system pole that controls the maximum gain for stability of the time delayed system. More will be said about stability in Section 3.3.

There is another way that the non-system poles affect the effectiveness of the time delayed velocity feedback control. We noticed the deterioration of the time delayed system's response (with negative velocity feedback) to the base acceleration shown in Figure 3(a) relative to that obtained by using the equivalent natural frequency and damping from the root locus plot from Figure 1. This degradation (see Figure 3(c) and 3(d)) is then due to the presence of these non-system poles. However, Figures 7(a) and 7(b) show that for $\tau = 1$, in the range of γ_v over which the equivalent damping is a maximum (see Figure 5), all these non-system poles have fairly large negative real parts. For example, at a gain of about 0.124, all the non-system poles have real parts less than about 0.17. While persistent excitations at the frequencies corresponding to the non-system poles could presumably cause large undesirable responses, such responses would, it appears, be far less significant for transient excitations such as those caused by strong earthquake ground shaking (see Section 4 for numerical results).

That these non-system poles indeed affect the response of a time delayed MDOF system has been shown both experimentally [15] and analytically [16]. Indeed, under steady-state sinusoidal

excitation, resonance phenomena are experimentally observed at frequencies corresponding to the non-system poles of a time-delayed system with velocity (integral, proportional) feedback, just as they are at frequencies corresponding to the system poles.

In the research literature to date, the presence of the non-system poles has been largely ignored presumably because the interest has been primarily on very small time delays, τ. However, even for small time delays, the time-delayed system's stability is affected by the presence of the non-system poles. When there is no time delay, the poles of an SDOF system with negative velocity feedback move leftwards as the gain is increased until they hit the real axis; they then travel in opposite directions along the real axis. The pole that moves (along the real axis) towards the origin, of course, never reaches the origin for any finite value of the control gain. When there is a time delay, things are substantially changed; no matter how small the time delay, a non-system pole enters the complex plane along the real axis from $-\infty$ when the gain is $\gamma_v = 0^+$, and moves rightward as the gain increases. This pole interacts with the system pole 'pushing' it root locus backwards as it were, and causing the system to become unstable at a certain value of the gain. We illustrate this in Figure 8(a) where we show the system pole of an SDOF system with a small time delay $\tau \simeq 0.0486$ being pushed back; this system pole then crosses the imaginary axis at a gain $\gamma_v \simeq 4.98$. Hence *ad hoc* rules [6,7], which state that the system is stable as long as the time delay, T_d is such that the ratio $T_\mathrm{d}/0.25T_n < 0.6$ lack rigor. In Figure 8(a), $\tau = T_\mathrm{d}/T_n \simeq 0.0486 \ll (0.6)(0.25) = 0.15$, and yet when the gain γ_v exceeds 4.98, the system becomes unstable. This cross-over of the system pole into the right half complex plane, even though the time delay is very small, is a consequence of its interaction with the non-system pole that travels rightward down the real axis as the gain is increased.

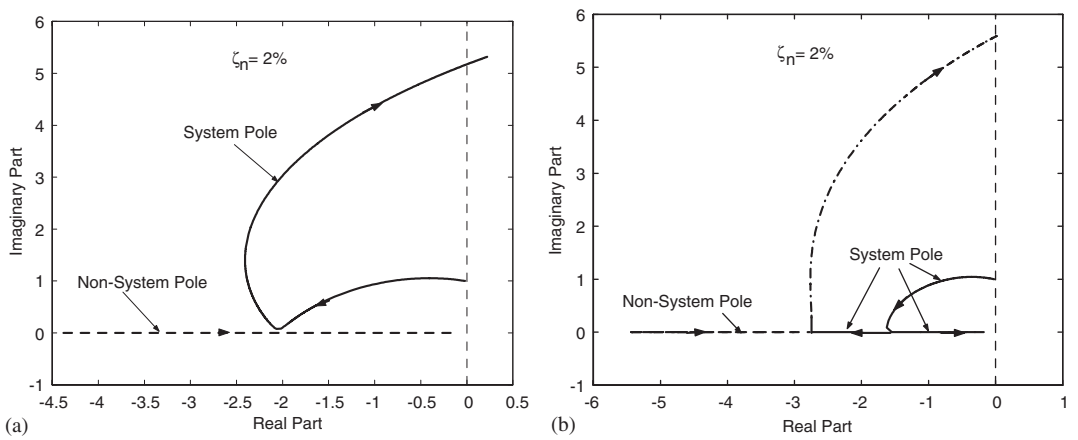

Figure 8. Upper half complex plane showing the interaction between the system pole (solid lines) and the non-system pole (dashed line). The arrows point in the direction of increasing gain γ_v. The gain for the system pole ranges from 0 to 5.5. (a) Root locus of the system pole for a time delay $\tau \approx 0.0485$. The pole starts very near the imaginary axis when the gain $\gamma_v = 0$, and swings downwards as the gain is increased. When the gain is about 1.336, it almost touches the real axis at an abscissa of about 2.04, but it is prevented from doing so by the non-system pole that is moving rightward and that has reached the same point at $\gamma_v \simeq 1.336$. The value of the gain at the left end of the root locus of the non-system pole is 1.2, and at its right end it is 5.5; and (b) root locus of poles for $\tau = 0.45$. Collision of the system and the non-system pole occurs at an abscissa of about 2.74, resulting in the root locus shown by the dash-dot line that crosses the imaginary axis at a gain of about 5.5.

In Figure 8(b) we show again the interaction of the system pole and the non-system pole for $\tau = 0.045$. Here, as before, the non-system pole travels rightwards along the real axis; the system pole reaches the real axis, and its branch that travels leftward along the real axis then 'collides' with the non-system pole coming in the opposite direction. This results in the root locus, shown by the dash-dot line, which turns backwards towards the imaginary axis, eventually crossing it as shown.

Lastly, we point out that the shape of the root loci of, what we have so far been calling, the 'system poles' in the vicinity of $\tau = 1$ is the consequence of a bifurcation that occurs through the interaction of the 'system pole' and a non-system pole. Hence non-system poles play a crucial and *unignorable* role in the dynamics of time delayed oscillatory systems, when the time delays are large. Figures 4(a–e) show that while the root loci of what we have called the system pole change gradually for values of $0.1 < \tau \leqslant 1$, there is a *qualitative* change in the shape of root loci that occurs for $1 \leqslant \tau \leqslant 1.1$ This qualitative change is caused by a bifurcation that occurs—a collision of the non-system pole with the system pole. This is depicted in Figures 9(a and b). As we increase the time delay from $\tau = 1$, we see at $\tau = \tau_b \simeq 1.015345$ an exchange of 'arms' between the root loci wherein the system pole exchanges its 'lower arm' for the 'upper arm' of the non-system pole. For value of $\tau > \tau_b$ the non-system pole having grabbed the lower arm of the system pole deflects downwards as the gain is increased; the system pole deflects upwards (see Figure 9b). For $\tau < \tau_b$, the non-system pole is deflected upwards as shown in Figures 7 and 9(a) as it attempts to 'run into' the system pole. It is because of this bifurcation that there is this sudden, *qualitative* change in the behavior of the system pole for $1 \leqslant \tau \leqslant 1.1$ observed in Figures 4(a–e). Thus, what we have been calling the root locus of the system pole is in fact not a pure system pole root locus in this range of τ values—it is actually a product of the interaction of the system pole with a non-system pole.

To get greater insight into these non-system poles we express Equation (17) as

$$R\left[1 - \frac{2\zeta_n}{R}\, e^{i\varphi} + \frac{1}{R^2}\, e^{2i\varphi}\right] = \gamma_v e^{i(\varphi - 2\pi\tau R\, \sin\varphi)} e^{2\pi\tau R\, \cos\varphi} \tag{27}$$

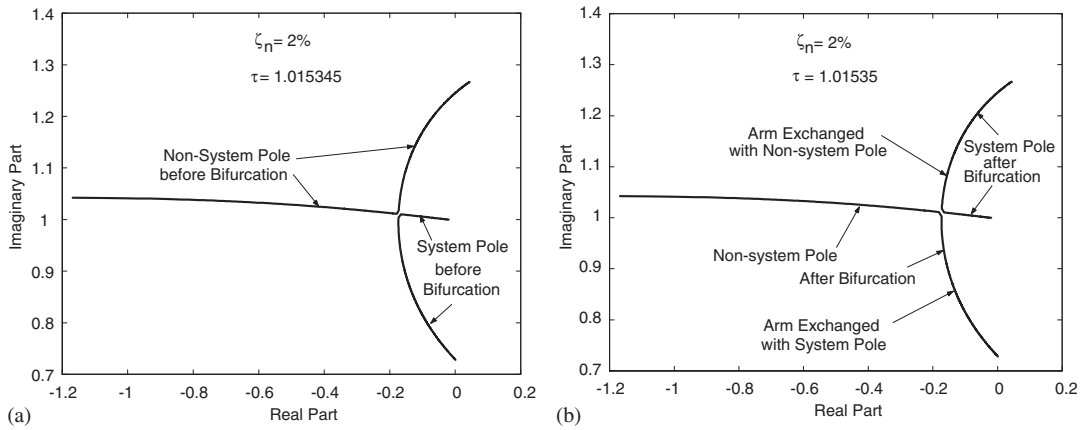

Figure 9. The qualitative change in the root loci of the so-called system pole for $1 \leqslant \tau \leqslant 1.1$ is caused by a bifurcation when the root loci of the system and the non-system poles interact and exchange 'arms' with one another.

Taking logarithms on both sides, we then find for $R \gg 1$ that

$$\ln(R) - \ln(\gamma_v) - 2\pi\tau R \cos\varphi - \frac{2\zeta_n}{R} e^{i\varphi} + \frac{1}{R^2} e^{2i\varphi} \simeq i(\varphi - 2\pi\tau R \sin\varphi \pm 2n\pi), \quad n = 0, 1, 2, \ldots \quad (28)$$

Taking the real part of Equation (28) gives

$$\ln(R) - \ln(\gamma_v) - 2\pi\tau R \cos\varphi - \frac{2\zeta_n}{R} \cos\varphi + \frac{1}{R^2} \cos 2\varphi \simeq 0 \quad (29)$$

which for $R \gg 1$, may be further simplified to

$$R \cos\varphi \simeq \frac{\ln(R) - \ln(\gamma_v)}{2\pi\tau} \quad (30)$$

Equation (30) gives us some insight into the root loci in Figure 7, since its left-hand side is just the magnitude of the real part of the pole. If we were to move along a vertical line in Figure 7, in going from one root locus to a higher one the value of R will increase, and so to keep $R\cos\varphi$ a constant (and thereby remain on the same vertical line), by Equation (30), the gain γ_v must increase. This feature is clearly observed for all the root loci for which R is large.

The last simplification of Equation (30) generated through the observation that $\ln(R) \ll R$ for $R \gg 1$, informs us that for very small gains $R\cos\varphi \approx O(1/2\pi\tau)$; the smaller the value of τ the farther left the non-system poles must lie in the complex $\tilde{s}$-plane for a given value of the gain.

As stated before, the lowest two root loci shown in Figure 7 behave somewhat differently from the above-mentioned general picture—not only is R not large for them, but they evince interaction with the system pole (see Figure 7). The lowest root locus appears to be retarded by the presence of the system pole; on the other hand, the root locus that is in line with the system pole appears to be accelerated rightwards for small values of the gain γ_v.

Similarly, taking the imaginary part of Equation (28) for $R \gg 1$ we obtain

$$2\pi\tau R \sin\varphi = \frac{2\zeta_n}{R} \sin\varphi - \frac{1}{R^2} \sin 2\varphi + \varphi \pm 2n\pi, \quad n = 0, 1, 2, \ldots \quad (31)$$

The ordinates, R, of the non-system poles when $\varphi = \pi/2$, that is, when the poles have reached the imaginary axis are obtained, for large R, from Equation (31) as

$$R = \left(\frac{2\zeta_n}{R} + \frac{\pi}{2} \pm 2n\pi\right)/2\pi\tau \simeq \frac{1}{\tau}\left[\frac{1}{4} + n\right], \qquad n = 0, 1, 2, \ldots \quad (32)$$

Equation (32) discloses that the approximate spacing between the root loci (the dashed lines) shown in Figures 7(a and b) for $R \gg 1$ is $1/\tau$! We thus see why the non-system poles are 'far away' when $\tau \ll 1$, compared with the system pole, which is in the vicinity of $R = 1$ when the damping factor and the gain are both small. And therefore these poles (except for the one that comes along the negative real axis) may not influence the transient response of the controlled structure. For example from Equation (32), when $\tau = 0.01$, we find that for $n = 1$ we get $R \simeq 100$. So the non-system poles occur at high frequencies at which the power in the input excitation would most likely be small, and the damping in the structure presumably high enough.

Each line of poles shown in Figures 7(a and b) is for a different value of n starting with the pole along the real axis for which $n = 0$. Also, as seen from Equation (32), the vertical locations of the dashed lines that represent the root loci are not much influenced by the uncontrolled systems damping factor as long as $\zeta_n \ll 1$. The smaller the value of τ, the larger the spacing between the successive root loci of the non-system poles.

The approximate values of γ_v at the corresponding values of R, for $R \gg 1$ at $\varphi = \pi/2$, are given by Equation (29) as

$$\gamma_v \simeq R \exp\left(-\frac{1}{R^2}\right) \leqslant R \simeq \frac{1}{\tau}\left[\frac{1}{4} + n\right], \qquad n = 0, 1, 2, \ldots \tag{33}$$

where we have used Equation (32) in the last equality. Equation (33) gives the approximate gains when each of the non-system poles (that have $R \gg 1$) cross the imaginary axis. To the best of our knowledge, Equations (32) and (33) give, for the first time, explicit results on the location of these non-system poles along with the corresponding values of the gains. From Equation (32) we observe that an infinite number of such poles exist, pointing to the infinite dimensionality of the time-delayed system.

The results provided by these equations are fairly accurate for non-system poles with $R \gg 1$. For example, numerical computations show that the uppermost non-system pole ($n = 10$) shown in Figure 7(a) intersects the imaginary axis when the gain $\gamma_v \simeq 10.153$, and that the ordinate when this pole crosses over is $R = 10.2506$. The corresponding estimates obtained from Equations (32) and (33) are $R = 10.25$, and $\gamma_v = 10.1529$. Similarly, for the third pole above the real axis ($n = 3$), numerical computation shows that it crosses the imaginary axis at an ordinate of 3.2522, while the estimate in Equation (32) gives a value of 3.25. The numerically computed value of γ_v when this crossover occurs is found to be 2.956, which is the same as the estimate provided by the first equality in Equation (33).

The study of these non-system poles leads us to the question of locating them accurately. Perhaps the most reliable way would be to use the argument principle. Denoting

$$w(\tilde{s}) = \tilde{s}^2 + 2\zeta_n \tilde{s} + 1 + \gamma_v \tilde{s} \exp(-2\pi\tau\tilde{s}) \tag{34}$$

the function $w(\tilde{s})$ maps any contour $\Gamma_{\tilde{s}}$ (traversed in the counter-clockwise direction) in the $\tilde{s}$-plane to a contour Γ_w in the w-plane. Since $w(\tilde{s})$ is an entire function, the number of zeros in any domain G enclosed by the contour $\Gamma_{\tilde{s}}$ that is traversed in the counter-clockwise direction in the complex $\tilde{s}$-plane equals the number of encirclements of the origin in the counter-clockwise direction (of the function $w(\tilde{s})$) by a point that moves along the mapped contour Γ_w in the w-plane [20]. We illustrate the use of this principle in Figures 10(a and b).

The values of the parameters chosen are $\zeta_n = 0.02, \tau = 1$, and $\gamma_v = 0.1$. The rectangular contour $\Gamma_{\tilde{s}}$ that is shown in Figure 10(a) is mapped into the w-plane depicted in Figure 10(b). The number of encirclements of the origin (whose location is shown by the asterisk) as seen in Figure 10(b) is three, indicating that we have three zeros of $w(\tilde{s})$ that lie within the rectangular region shown in Figure 10(a) for these parameter values. This is confirmed by the root loci shown in Figure 7(a).

As numerically verified above, Equations (32) and (33) appear to be fairly accurate approximations that provide the locations in the $\tilde{s}$-plane at which the non-system poles intersect the imaginary axis (along with the corresponding values of the gains) when the values of $R \gg 1$. However for smaller values of R, the best way to locate the non-system poles is through the use of the argument principle illustrated in Figure 10. This is especially so for the non-system poles with small R (say, $R < 2$) in the $\tilde{s}$-plane, because these poles, in addition, may interact with the system poles (see Figure 9), and such interactions are not considered in obtaining Equations (32) and (33).

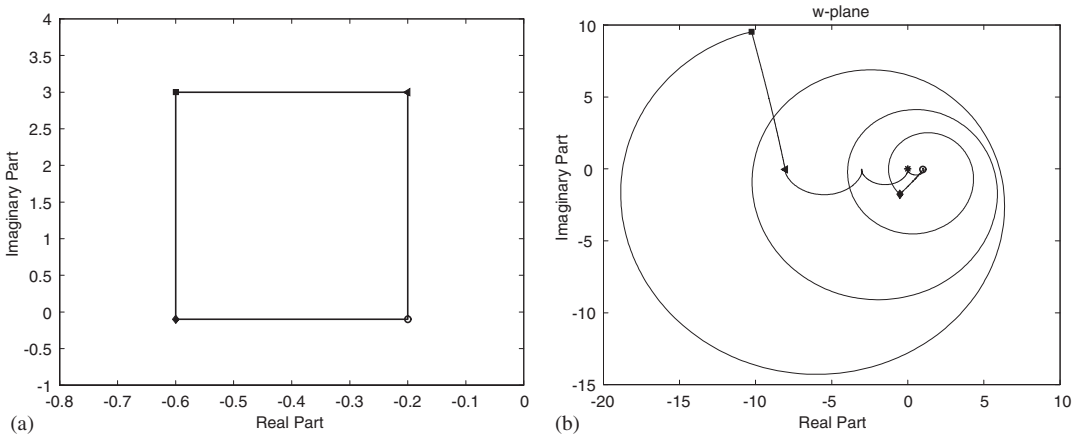

Figure 10. (a) The contour $\Gamma_{\tilde{s}}$ in the $\tilde{s}$-plane is shown by the rectangle; and (b) the function $w(\tilde{s})$ in the w-plane as the contour $\Gamma_{\tilde{s}}$ is traversed in the $\tilde{s}$-plane (in the counter-clockwise direction). The parameters chosen are $\zeta_n = 0.02$, $\tau = 1$, and $\gamma_v = 0.1$. The origin in the w-plane is marked by an asterisk. The number of counter-clockwise rotations about the origin in the w-plane gives the number of zeros of the function $w(\tilde{s})$ that lie inside the contour $\Gamma_{\tilde{s}}$.

3.3. Stability of poles

Here we look at the maximum gain for stability for the time-delayed system, considering both system and non-system poles. Though this has been looked at for both proportional and velocity feedback time-delayed control [6,7], our attention will be on time delays that can be large ($O(T_n)$), and for both positive and negative velocity feedback, time-delayed control. Results of previous investigators will be shown to be a subset of the results that we obtain here.

The maximum gain for stability corresponding to the system poles for a given value of the time delay τ is obtained by noticing that when the time-delayed system is marginally stable, its poles $\tilde{s}_{1,\bar{1}}(\tau, \gamma_v)$ lie on the imaginary axis. Hence setting $\tilde{s} = ir_c = i\omega_c/\omega_n$ in Equation (6), where ω_c is the (real) cross-over frequency at which the system pole of the time-delayed system lies on the imaginary axis and is about to cross over into the right half complex $\tilde{s}$-plane, we get the two relations

$$r_c^2 - r_c\gamma_v \sin(2\pi\, r_c\tau) - 1 = 0 \tag{35}$$

and

$$r_c[\gamma_v \cos(2\pi\, r_c\tau) + 2\zeta_n] = 0 \tag{36}$$

The quantity r_c is the dimensionless cross-over frequency. Hence, the poles of the velocity feedback system with a given time delay τ cross over into the right half complex plane at a dimensionless frequency r_c that must satisfy the relation (note that $r_c = 0$, does not satisfy Equation 35)

$$\cos(2\pi r_c\tau) = -\frac{2\zeta_n}{\gamma_v} \tag{37}$$

Since $|\cos(2\pi r_c\tau)| \leqslant 1$, the system is stable for all gains g_v for which $|\gamma_v| < 2\zeta_n$. In this range of gains, the system, *irrespective of whether we use positive or negative feedback*, will always be

stable for all values of the time delay τ. Note that when $\gamma_v > 0$ we have negative feedback, and when $\gamma_v < 0$ we have positive feedback. We now consider the following cases when $|\gamma_v| \geqslant 2\zeta_n$.

3.3.1. Time-delayed negative velocity feedback.

(a) When $\gamma_v = 2\zeta_n$, from Equation (37), $\cos(2\pi r_c \tau) = -1$, and hence $r_c\tau = (2n+1)/2$, $n = 0, 1, 2, \ldots$. Equation (35) then gives $r_c = \pm 1$.
(b) When $\gamma_v > 2\zeta_n$, Equation (37) gives $r_c\tau = n + \theta/2\pi$, and $r_c\tau = (n+1) - \theta/2\pi$, $n = 0, 1, 2, \ldots$, where the angle $\pi/2 \leqslant \theta \leqslant \pi$ is given by $\theta = \cos^{-1}(-2\zeta_n/\gamma_v)$.

The dimensionless cross-over frequencies corresponding to $r_c\tau = n + \theta/2\pi$ can be obtained now using Equation (35) as

$$r_c^{(1)}(\gamma_v, \zeta_n) = \frac{1}{2}\left[\sqrt{\gamma_v^2 - 4\zeta_n^2} \pm \sqrt{\gamma_v^2 + 4(1-\zeta_n^2)}\right] \tag{38}$$

Similarly, the cross-over frequencies corresponding to $r_c\tau = (n+1) - \theta/2\pi$ can be obtained as

$$r_c^{(2)}(\gamma_v, \zeta_n) = \frac{1}{2}\left[-\sqrt{\gamma_v^2 - 4\zeta_n^2} \pm \sqrt{\gamma_v^2 + 4(1-\zeta_n^2)}\right] \tag{39}$$

Since the zeros of Equation (6) come in complex conjugate pairs, we shall deal with the upper half complex plane, and so concern ourselves with only the positive sign before the radical in Equations (38) and (39).

Another interpretation of the above equations would be that for a given gain $\gamma_v > 2\zeta_n$, the cross-over could occur at the dimensionless frequency $r_c^{(1)}$, and at a time delay given by

$$\tau_n^{(1)}(\gamma_v, \zeta_n) = \frac{2\pi n + \theta}{2\pi r_c^{(1)}}, \qquad n = 0, 1, 2, \ldots \tag{40}$$

where $r_c^{(1)}$ is given by Equation (38), with the positive sign chosen for the radical. It could also occur at a dimensionless frequency of $r_c^{(2)}$ and a corresponding time delay of

$$\tau_n^{(2)}(\gamma_v, \zeta_n) = \frac{(2n+2)\pi - \theta}{2\pi r_c^{(2)}}, \qquad n = 0, 1, 2, \ldots \tag{41}$$

where $r_c^{(2)}$ is given in Equation (39), with the positive sign chosen for the radical. Therefore, for a given $\gamma_v > 2\zeta_n$, the system first becomes unstable for a dimensionless time delay τ_u given by

$$\tau_u(\gamma_v, \zeta_n) = \min_{\forall n} [\tau_n^{(1)}, \tau_n^{(2)}] \tag{42}$$

We then observe that the dimensionless time delay τ_u at which the system poles cross into the right half plane is a function of the dimensionless gain γ_v and the damping factor ζ_n of the uncontrolled system.

Let us consider the behavior of $\tau_n^{(1)}$ and $\tau_n^{(2)}$ as functions of γ_v for any fixed, given value of $\zeta_n = \zeta_{n0}$. Then when $\gamma_v = 2\zeta_{n0}$, from Equations (38) and (39) we obtain $r_c^{(1)} = r_c^{(2)} = 1$; also, from Equation (37) we obtain $\theta = \pi$, so that

$$\tau_n^{(1)}(\gamma_v = 2\zeta_{n0}, \zeta_n = \zeta_{n0}) = \tau_n^{(2)}(\gamma_v = 2\zeta_{n0}, \zeta_n = \zeta_{n0}) = \frac{2n+1}{2}, \qquad n = 0, 1, 2, \ldots \tag{43}$$

Hence, for any given value of $\zeta_n = \zeta_{n0}$ the curves $\tau_n^{(1)}$ and $\tau_n^{(2)}$, considered as function of γ_v, meet at $\gamma_v = 2\zeta_{n0}$. Equation (43) constitutes a generalization of the result we obtained earlier in

Equation (16) under the assumption that $\tau = 1/2$ and $\tau\zeta_{n0} \ll 1$. We shall show later on a similar general result for time-delayed positive velocity feedback also (see Equation 46).

Furthermore, for $\gamma_v > 2\zeta_{n0}$ the two sets of curves, $\tau_{n+1}^{(1)}$ and $\tau_n^{(2)}$ (again, for any given value of $\zeta_n = \zeta_{n0}$, and so considered as functions of γ_v) intersect one another (note that $r_c^{(2)} \leqslant r_c^{(1)}$). Their intersection points are given by those values of γ_v that satisfy the relation

$$\cos\left(\frac{2(n+1)\pi\sqrt{\gamma_v^2 - 4\zeta_{n0}^2}}{\sqrt{\gamma_v^2 + 4(1-\zeta_{n0}^2)}}\right) + \frac{2\zeta_{n0}}{\gamma_v} = 0 \tag{44}$$

3.3.2. Time-delayed positive velocity feedback.

(a) When $\gamma_v = -2\zeta_n$, from Equation (37), $\cos(2\pi r_c\tau) = 1$, and hence $r_c\tau = n, \quad n = 0, 1, 2, \ldots$. Equation (35) then gives $r_c = \pm 1$.

(b) When $\gamma_v < -2\zeta_n$, a similar analysis yields the expressions

$$\tau_n^{(1)}(\gamma_v, \zeta_n) = \frac{\theta + 2\pi n}{2\pi r_c^{(2)}}, \quad n = 0, 1, 2, \ldots \tag{45}$$

and

$$\tau_n^{(2)}(\gamma_v, \zeta_n) = \frac{(2n+2)\pi - \theta}{2\pi r_c^{(1)}}, \quad n = 0, 1, 2, \ldots \tag{46}$$

where $r_c^{(1)}$ and $r_c^{(2)}$ are given in Equations (38) and (39) respectively, and $0 \leqslant \theta \leqslant \pi/2$. As before, the time delay, τ_u, at the crossover of the system pole is given by

$$\tau_u(\gamma_v, \zeta_n) = \min_{\forall n}[\tau_n^{(1)}, \tau_n^{(2)}] \tag{47}$$

We consider the functions $\tau_n^{(1)}(\gamma_v, \zeta_n)$ and $\tau_n^{(2)}(\gamma_v, \zeta_n)$ for any given specific value of the damping factor. For such a value, $\zeta_n = \zeta_{n0}$, when $\gamma_v = -2\zeta_{n0}$ we obtain from Equations (38) and (39) that $r_c^{(1)} = r_c^{(2)} = 1$; also, from Equation (37) we obtain $\theta = 0$, so that

$$\tau_{n+1}^{(1)}(\gamma_v = 2\zeta_{n0}, \zeta_n = \zeta_{n0}) = \tau_n^{(2)}(\gamma_v = 2\zeta_{n0}, \zeta_n = \zeta_{n0}) = n + 1, \qquad n = 0, 1, 2, \ldots \tag{48}$$

Hence, for any given value of $\zeta_n = \zeta_{n0}$ the curves $\tau_{n+1}^{(1)}$ and $\tau_n^{(2)}$, considered as function of γ_v, meet at $\gamma_v = -2\zeta_{n0}$. Likewise for any given value of $\zeta_n = \zeta_{n0}$, and $\gamma_v < -2\zeta_{n0}$ the curves for $\tau_n^{(1)}$ and $\tau_n^{(2)}$ given by Equations (45) and (46), respectively, may be taken to be functions of the dimensionless gain γ_v. These curves intersect, and their points of intersection satisfy the relation

$$\cos\left(\frac{(2n+1)\pi\sqrt{\gamma_v^2 - 4\zeta_{n0}^2}}{\sqrt{\gamma_v^2 + 4(1-\zeta_{n0}^2)}}\right) - \frac{2\zeta_{n0}}{\gamma_v} = 0 \tag{49}$$

We show these results pictorially in Figure 11 where we have taken the damping factors of $\zeta_{n0} = 0.02$ and 0.05. The curves for $\tau_n^{(1)}$ and $\tau_n^{(2)}$ as functions of γ_v are shown for both positive and negative feedback. The intersections of these two families of curves given by the smallest roots γ_v of Equations (44) and (49), delimit the region of stability; they are shown by the solid circles at each intersection. The system poles are stable for all points (γ_v, τ) that lie in the region between the scallop-shaped solid lines as indicated in the figure. As τ increases, the region of stability narrows.

Figure 11(a) shows that for time-delayed negative velocity feedback with $\tau = 1$, and $\zeta_n = 0.02$ the maximum gain to ensure stability is $\gamma_v = 0.4737$. From our discussion in the previous section, we know that this pertains to the crossing of one of the *non-system* poles across the imaginary axis; and so, stability here is not controlled by the 'system pole'. Our root locus for this non-system pole gives precisely this value of this gain at the cross-over, as we saw in the last section.

Figure 12 shows the cross-over frequency versus time delay for $\zeta_n = 0.02$ using time-delayed, negative and positive velocity feedback. These are the cross-over frequencies that correspond to the maximum gains for stability shown in Figure 11(a). Figure 13 shows similar results for

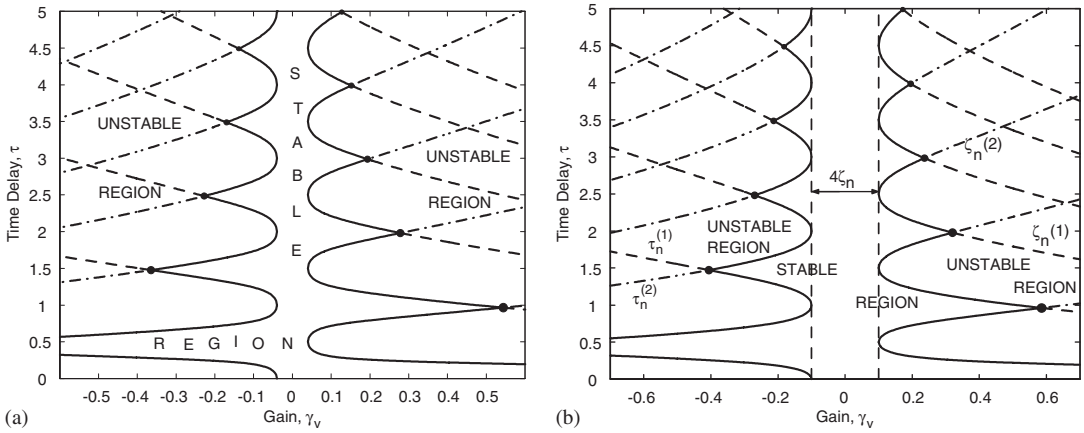

Figure 11. (a) Zones of stability for $\zeta_n = 2\%$; and (b) zones of stability for $\zeta_n = 5\%$. Notice the stable regions around $\tau \simeq n$ for negative velocity feedback (and around $\tau \simeq (2n+1)/2$, for *positive* velocity feedback), $n = 0, 1, 2, \ldots$. The curves beyond the stable region of the set $\{\tau_n^{(1)}\}_{n=1}^{n=5}$ are shown by dashed lines, those of the set $\{\tau_n^{(2)}\}_{n=1}^{n=5}$ are shown by dash-dot lines. The region between the dark scallop-shaped solid lines is stable.

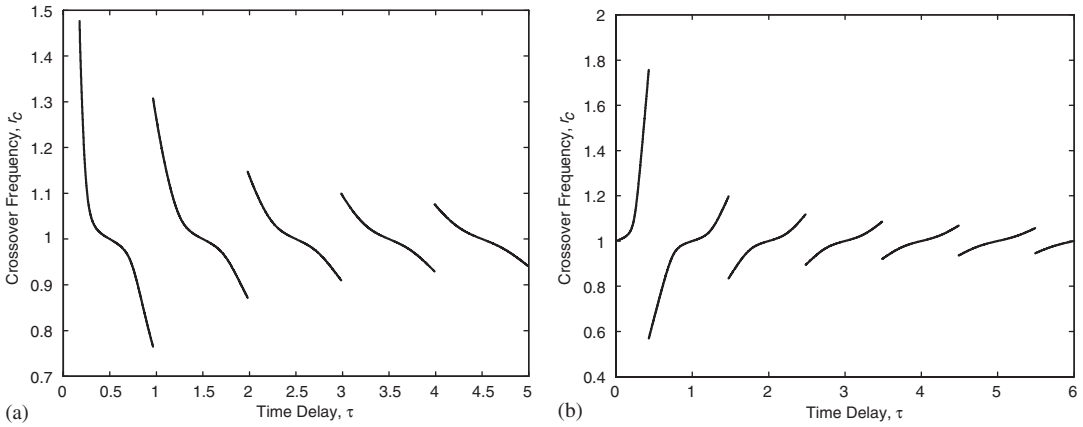

Figure 12. Cross-over frequency versus time delay for $\zeta_n = 2\%$: (a) using time delay with negative velocity feedback; and (b) using time delay with positive velocity feedback.

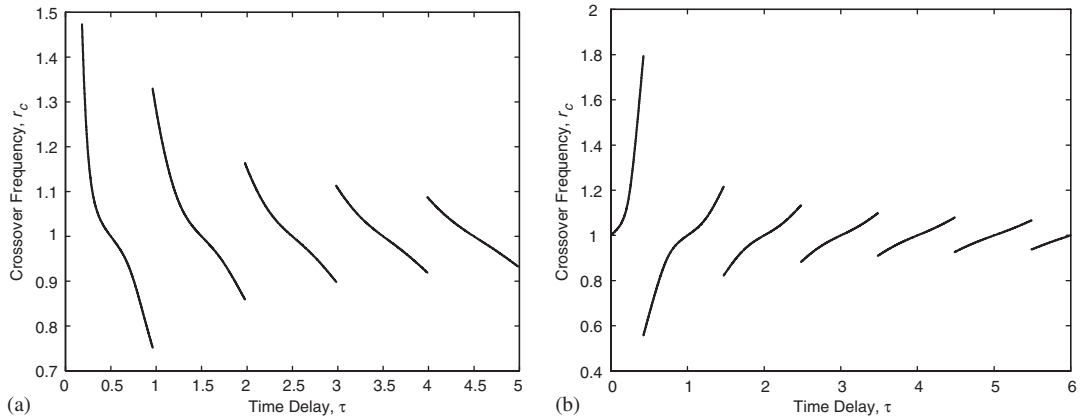

Figure 13. Cross-over frequency versus time delay for $\zeta_n = 5\%$: (a) using time delay with negative velocity feedback; and (b) using time delay with positive velocity feedback.

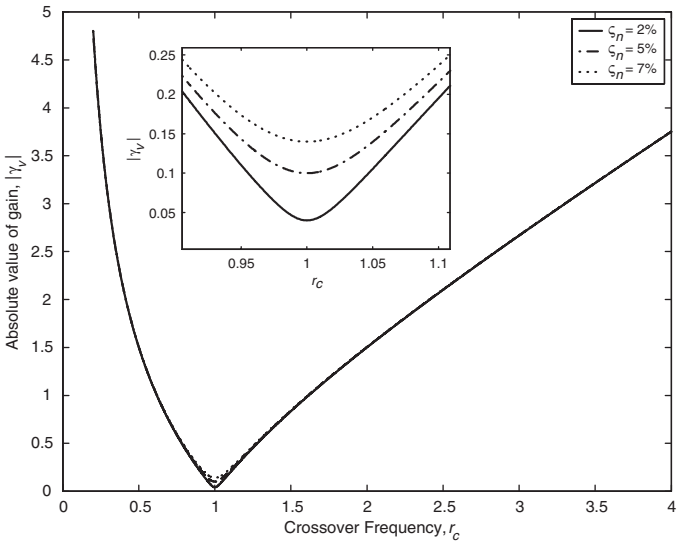

Figure 14. Graph showing absolute value of the gain ($|\gamma_v|$) versus cross-over frequency (r_c) for different damping ratios (ζ_n). If a cross-over occurs for a frequency r_c, then the gain, $|\gamma_v|$, is given by the graph.

$\zeta_n = 0.05$ that correspond to the maximum gains for stability shown in Figure 11(b).

From Equation (6), a necessary condition for cross-over is

$$|\gamma_v| = \frac{|-r_c^2 + 2\zeta_n r_c i + 1|}{r_c}$$

This equation relates the absolute value of the gain at cross-over $|\gamma_v|$ to the crossover frequency r_c and the damping ratio ζ_n. Note that this relation is independent of time delay. Figure 14 shows a plot of the absolute value of the gain at cross-over versus crossover frequency for different damping ratios. As seen from the plot, the damping ratio appears to have a

significant effect on the shape of the plot only for values of r_c in the vicinity of unity; also, for a given value of $|\gamma_v|$ there can be at most two cross-over frequencies, irrespective of the value of the time delay, τ.

In addition to giving an understanding of stability issues in time-delayed systems, Figures 11–14 can also be used for the design of time-delayed systems that employ both negative and positive velocity feedback.

4. APPLICATION OF CONTROL DESIGN PRINCIPLES TO MDOF SYSTEMS

4.1. Multi-actuator, multiple time-delayed velocity feedback control of MDOF systems

In this section we shall apply the principles that we developed in the last two sections to time-delayed velocity feedback control of multi-degree-of-freedom system, assuming that that the system is classically damped. Our system can then be described by the equation

$$M\ddot{x} + C\dot{x} + Kx = f(t) \tag{50}$$

where we shall take M and K to be n by n positive-definite matrices, and the force vector $f(t)$ on the right-hand side can be appropriately taken when one wants to determine the response of such a system to a base excitation, such as caused by strong earthquake ground shaking. Using the transformation

$$x = Pz \tag{51}$$

where

$$P^{\mathrm{T}}MP = I \tag{52}$$

$$P^{\mathrm{T}}KP = \mathrm{Diag}(\omega_1^2, \omega_2^2, \ldots, \omega_n^2) \tag{53}$$

and

$$P^{\mathrm{T}}CP = \mathrm{Diag}(2\zeta_1\omega_1, 2\zeta_2\omega_2, \ldots, 2\zeta_n\omega_n) \tag{54}$$

we obtain the response of each mode to be

$$\ddot{z}_i + 2\omega_i\zeta_i\dot{z}_i + \omega_i^2 z = q_i(t), \qquad i = 1, 2, \ldots, n \tag{55}$$

where z_i is the ith component of the vector z, and q_i is the ith component of the vector $q = P^{\mathrm{T}}f(t)$. The natural period of the ith mode is then given by $T_i = 2\pi/\omega_i$. We can use time-delayed velocity feedback control to reduce the response of one or more modes, as desired, by using a control force given by

$$\ddot{z}_i + 2\omega_i\zeta_i\dot{z}_i + \omega_i^2 z = q_i(t) - g_i\dot{z}_i(t - T_{\mathrm{d}i}), \qquad i = 1, 2, \ldots, n \tag{56}$$

Thus to control the ith mode we use a velocity signal that is time-delayed by $T_{\mathrm{d}i} \simeq T_i$. For each value of the damping factor, plots such as those shown in Figures 5(a) and 5(b) can be used to give the proper gains g_i to be used. As seen from these Figures one would most likely want to use those values of the gains that maximize the equivalent damping factors. Note that dimensionless plots like those in Figure 5 *do not* depend on the value of ω_i; they depend only on the damping factor of the uncontrolled mode ζ_i. The values of the modal gains are $g_i = \gamma_v\omega_i$ (see relations following Equation 6), where, for each mode, γ_v is appropriately chosen using such figures. The

values of the chosen gains determine the magnitudes of the control forces that would be called for in performing active structural control. Whether they can be applied, from a practical standpoint, depends on various design constraints. Among them are the characteristics of the actuators to be deployed, and economic considerations. Assuming that these constraints can be satisfied, we can then rewrite the control system, in terms of the physical coordinates as

$$M\ddot{x} + C\dot{x} + Kx = f(t) - \sum_{i=1}^{i=n} G_i \dot{x}(t - T_{\mathrm{d}i}) \tag{57}$$

with $T_{\mathrm{d}i} \simeq T_i$. Here the gain matrices G_i are given by

$$G_i = PD_iP^{\mathrm{T}} \tag{58}$$

where D_i is a diagonal matrix whose elements are all zero except for the ith column element, which is g_i. If the jth mode is not to be controlled—and this may depend on the frequency content of the force, $f(t)$; the fact that higher modes may have larger damping; and difficulties in

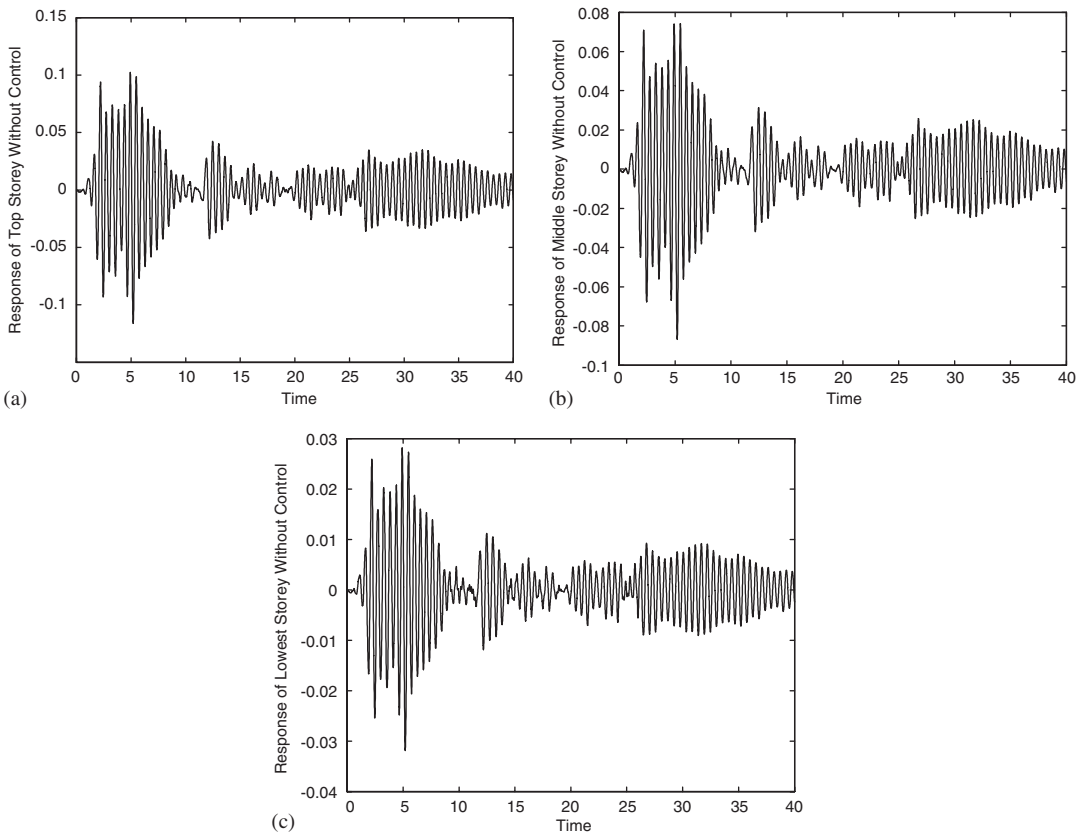

Figure 15. Response of the three-storey structure to the S00W component of the El Centro 1940 base acceleration.

the practical implementation of very small time delays—then, $g_j = 0$, and the jth term drops out of the summation in Equation (57).

Notice that we have expanded the usual time-delayed control system developed to date that generally uses a *single* time delay and created one that has *multiple time delays*. This extension is required because each mode requires a different time delay to address both performance and stability issues (as seen in Sections 3.1 and 3.3) in an effective manner. Also, notice that our control scheme is non-colocated and requires distributed control.

4.2. Numerical results

We consider here a building structure modeled as a 3-DOF system whose stiffness matrix K is given by

$$K = \begin{bmatrix} 500 & -500 & 0 \\ -500 & 1000 & -500 \\ 0 & -500 & 1500 \end{bmatrix} \tag{59}$$

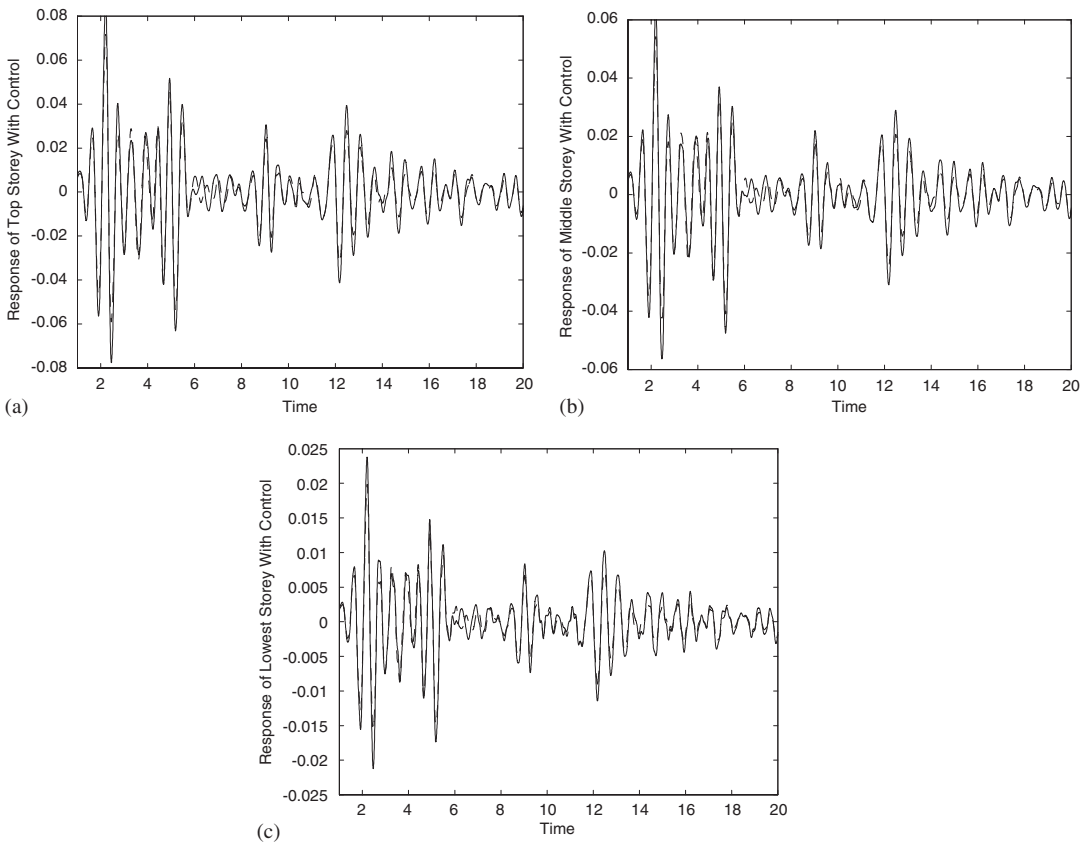

Figure 16. Comparison of the response during large amplitude response of the three-storey structure using time-delayed velocity feedback (solid line) and direct velocity feedback with no time delay (dashed line).

(in suitable units), whose mass matrix is the 3×3 identity matrix, and whose damping factors for the first, second, and third mode are, respectively, 0.02, 0.05, and 0.1. The periods of vibration of the three modes are $T_1 \simeq 0.54$ s, $T_2 \simeq 0.2$ s, and $T_3 \simeq 0.15$ s. The base acceleration that the structure is subjected to is the S00E component of the El Centro earthquake of 1940.

We assume that there are large time delays prevalent in the control loop that are difficult to eliminate/nullify, and so we shall explore the introduction of intentional time delays to control the system. As with any control design, we are interested in both performance and stability. We illustrate the design principles developed in this paper through this numerical example.

Choice of time delays and control gains for each mode of vibration: One way of carrying out the time-delayed control design is to look at the modes of the system and attempt to control them. Since the third mode has considerable damping, we shall attempt to control only the lower two modes of vibration of the system. To do this we use time delays of $T_{d1} = T_1$ s and $T_{d2} = T_2$ s

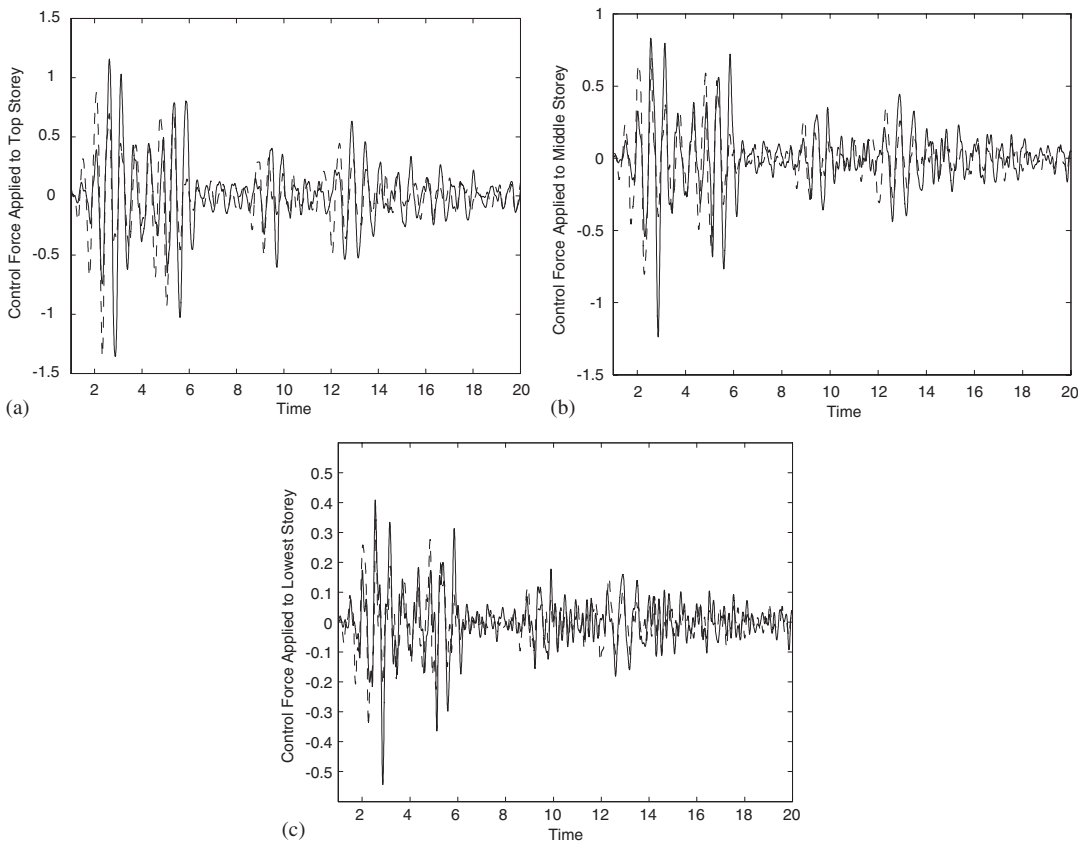

Figure 17. Comparison during large-amplitude response of the control force required (at each storey) using time-delayed velocity feedback control (solid line) and direct velocity feedback with no time delay (dashed line).

for the two modes that we want to control. In order to have good performance, we select from Figure 5 those gains for which the time-delayed system modes show the largest equivalent damping factors; for the first mode we use $\gamma_v = 0.124$, and for the second mode, $\gamma_v = 0.106$. We next check stability and sensitivity of the control system to variations in the time delay parameters. Figure 11(a) shows that with this gain ($\gamma_v = 0.124$) the first mode (with damping factor 0.02) is stable for time delays ranging from $0.75T_1 \simeq 0.4$ s to $1.2T_1 \simeq 0.64$ s; similarly with a gain of 0.106, as seen from Figure 11(b), the second mode will be stably controlled as long as the time delay is maintained between $0.57T_2 \approx 0.12$ s and $1.41T_2 \simeq 0.28$ s. The gains $g_1 = \gamma_v\omega_1 \simeq 1.4353$ and $g_2 \approx 3.3520$ are then employed along with the respective time delays for the two modes that are controlled using time-delayed velocity feedback. The third mode is left uncontrolled.

The matrices G_1 and G_2 in Equation (58) become

$$G_1 = \begin{bmatrix} 0.8927 & 0.6535 & 0.2392 \\ 0.6535 & 0.4784 & 0.1751 \\ 0.2392 & 0.1751 & 0.0641 \end{bmatrix} \quad \text{and} \quad G_2 = \begin{bmatrix} 1.1173 & -1.1173 & -1.1173 \\ -1.1173 & 1.1173 & 1.1173 \\ -1.1173 & 1.1173 & 1.1173 \end{bmatrix} \tag{60}$$

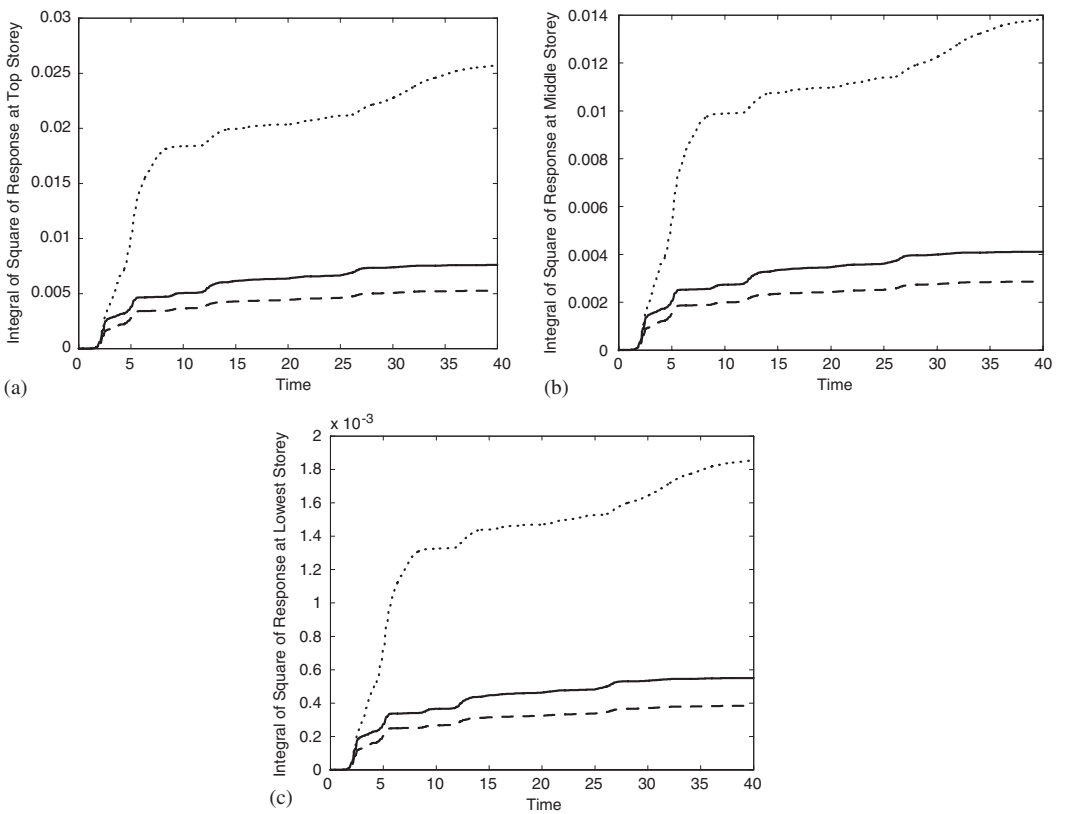

Figure 18. Integral of square of response (at each storey) using time-delayed control (solid line) and velocity feedback control (dashed line) during time-history of motion. The dotted line shows the integral of the square of the uncontrolled response.

Figures 15(a–c) show the uncontrolled response of the structure to the earthquake ground motion. Figures 16(a–c) show a comparison of structural response (during the large-amplitude motions) when using direct velocity feedback with no time delay (dashed line), and our time-delayed velocity feedback control design (solid line). In each case, for comparison, the same gains are used for each mode with and without time delay. We observe that though the response with direct velocity feedback is slightly smaller that with the time delay design, the difference is not very substantial.

Figure 17(a–c) shows the control force that needs to be exerted at each storey using time-delayed control (solid line) and compares it with that needed for velocity feedback control with no time delay(dashed line). We see that our time-delayed control design requires somewhat larger forces to be applied than for direct velocity feedback. Figure 18(a–c) shows the integral of the square of the response using no control (dotted line), velocity feedback control (dashed line), and time-delayed velocity feedback control (solid line). This figure again shows that though not as efficient as direct velocity feedback, time-delayed

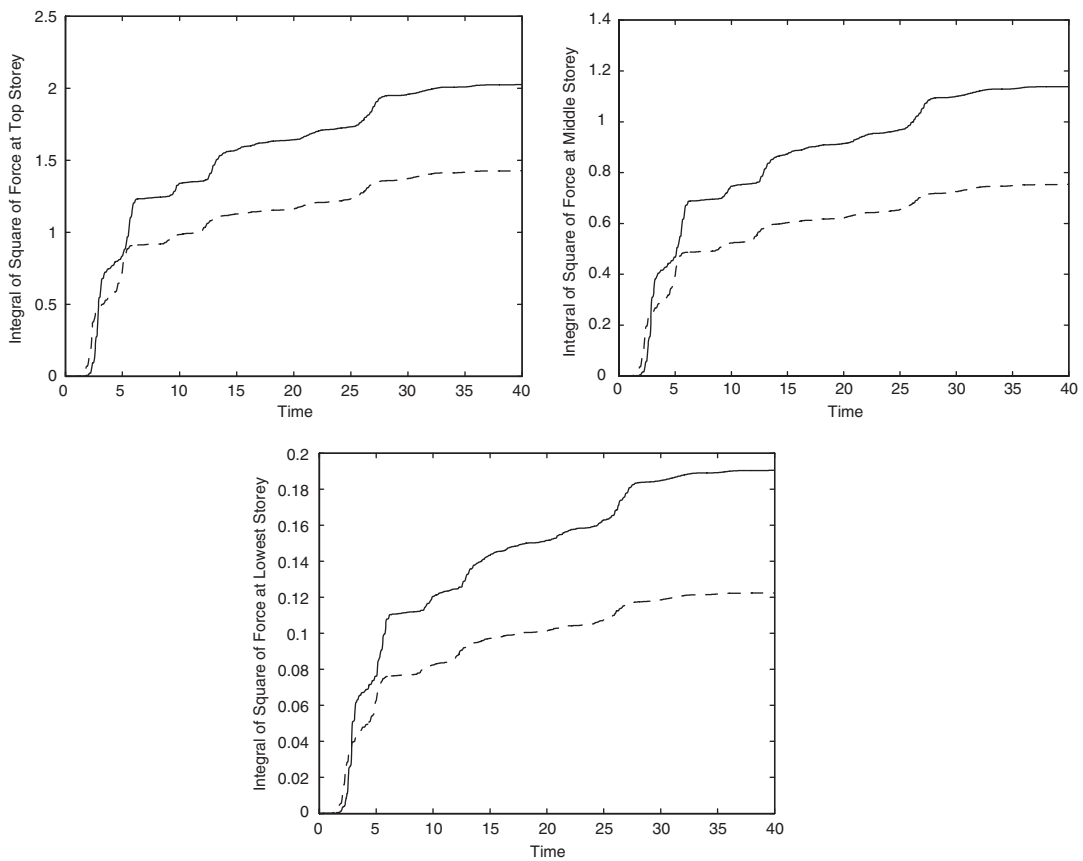

Figure 19. The integral of the square of the control force (at each storey) required using the time-delayed control design (solid line) and that required using velocity feedback (dashed line).

control is still very effective in absorbing the energy of the structure, and reducing its rms amplitude. Lastly, in Figure 19(a–c) we compare the integral of the square of the control force at each storey for velocity feedback and time-delayed velocity feedback. We see that the energy spent in performing time-delayed control is about 30% higher at the top storey than that required using velocity feedback control. Though at the lower stories this percentage increases, the magnitudes of the forces involved are much smaller at these levels (see Figures 19b and c). We thus see that time-delayed control is stable, and its performance effective.

Similar results are obtained for the synthetically generated base acceleration displayed in Figure 3(a) that uses a randomly generated time series multiplied by an envelop function. They confirm our analysis that the time-delayed control though only slightly inferior to direct velocity feedback, gives us the flexibility to design controllers that can utilize the presence of inherent (large) time delays in structural control.

5. CONCLUSIONS

There are always time delays in the control loop for the active control of structural systems. One strategy for dealing with such time delays is to try to eliminate/nullify their effect; however, such a strategy may not be always useable, especially when the delays become large when compared with the natural periods of vibration of the system. An alternative strategy—especially useful when the delays are large and cannot be easily compensated/eliminated/nullified—is to develop control design principles that incorporate time delays in the control loop, and so attempt to use the delays to advantage, when possible. This paper explores this latter strategy and develops design principles for the time-delayed control of vibratory systems. As such, these principles are equally applicable to civil, aerospace, mechanical, chemical, and process control systems in which significant time delays in the control loop may be unavoidable.

The paper considers both performance and stability issues in the design of time-delayed velocity feedback control of MDOF systems. We show that at time delays close to the fundamental period of an SDOF system the equivalent damping factor, as determined from the system poles, is high. This translates into performance-related design principles which we subsequently use in the time-delayed control of MDOF systems. We show the presence and interaction of non-system poles with the system poles. The presence of these non-system poles has been largely ignored in studies of active control to date. We show that they cannot be ignored in the development of design principles dealing with large time delays for they affect both the stability as well as the performance of the control design. We obtain explicit expressions for the location of these non-system poles and show that in general there are an infinite number of them. We develop a general and detailed stability analysis for SDOF systems with both positive and negative time-delayed velocity feedback. All our results are valid for large time delays. They go beyond—include, and correct—some of the results hereto developed for systems with small time delays. This analysis then translates into stability-related design principles for MDOF systems.

The paper contains several basic results. It systematically studies the effect of non-system poles, gives explicit expressions regarding their location (along with the corresponding values of the gains), and shows their central importance in understanding the behavior of time-delayed

control systems. It is shown that even the 'system poles,' for time delays that are comparable to the natural period of an SDOF system, can actually be a consequence of interaction with the non-system poles. The non-system poles are shown to influence both system stability and system performance and cannot therefore be ignored in such control designs.

Using this basic understanding, we provide one possible control design methodology for classically damped MDOF systems using multiple actuators and multiple time delays. A numerical example of a building structure modeled as a three-degree-of-freedom system that is subjected to the El Centro 1940 S00W earthquake record is considered. We see that the time-delayed control that we obtain, though obviously not as efficient as direct velocity feedback, is effective in controlling the system while still being amply stable.

Any control design—and indeed any design—is both an art and a science. It is situation specific, and depends on various constraints, such as the force capacity of the actuator, its bandwidth, the structural properties of importance, and the extent of delay in the control loop. Whether one might want to use time-delayed active control in a structure (as proposed herein) or some other manner of control is likewise contingent on numerous considerations, not the least of which may be those that are economic. This paper explores a new and different strategy for the control of structures for which the time delays in the control loop may be large and difficult to eliminate. We hope this work opens up new avenues of research and practice in the active control of structures. As such, it constitutes only a beginning.

REFERENCES

1. Satche M. Stability of linear oscillating systems with constant time lag. *Journal of Applied Mechanics* 1949; **16**: 419–420.
2. Choksy NH. Time lag systems. *Progress in Control Engineering* 1962; **1**:17–38.
3. Abdel-Rohman M. Structural control considering time delays. *Transactions of the Canadian Society for Mechanical Engineering* 1985; **9**:224–227.
4. Abdel-Rohman M. Time delays effects on actively damped structures. *Journal of Engineering and Mechanics* (ASCE) 1987; **113**:1709–1719.
5. Sain PM, Spencer BF, Sain MK, Suhardjo J. Structural control design in the presence of time delays. *Proceedings of the 9th Engineering Mechanics Conference,* ASCE, College Station, 24–27 May, 1992.
6. Agarwal AK, Fujino Y, Bhartia B. Instability due to time delay and its compensation in active control of structures. *Earthquake Engineering and Structural Dynamics* 1993; **22**:211–224.
7. Agarwal AK, Yang JN. Effect of fixed time delay on stability and performance of actively controlled civil engineering structures. *Earthquake Engineering and Structural Dynamics* 1997; **26**:1169–1185.
8. Agarwal AK, Yang JN. Compensation for time delay for control of civil engineering structures. *Earthquake Engineering and Structural Dynamics* 2000; **29**:37–62.
9. Marshall JE. Extensions of O.J. Smith's method to digital, other systems. *International Journal of Control* 1974; **19**: 933–939.
10. Udwadia FE, Kumar R. Time delayed control of classically damped structural systems. *International Journal of Control* 1994; **60**:687–713.
11. Udwadia FE. Noncollocated point control of nondispersive continuous systems using time delays. *Applied Mathematics and Computation* 1991; **42**(1):23–63.
12. Udwadia FE. Noncollocated control of continuous systems with tip-inertias. *Applied Mathematics and Computation* 1992; **47**:47–75.
13. Udwadia FE, Kumar R. Time delayed control of classically damped structures. *Proceedings of the 11th World Conference on Earthquake Engineering*, Acapulco, Mexico, 23–28 June, 1994.
14. von Bremen H. Udwadia FE. Can time delays be useful in the control of structural systems? *Proceedings of the 42nd AIAA/ASME/ASCE/AHS Structures, Dynamics and Materials Conference*, Atlanta, 3–6 April, 2000.
15. von Bremen H, Udwadia FE. Effect of time delay on the control of a torsional bar. *Proceedings of the 43nd AIAA/ASME/ASCE/AHS Structures, Dynamics and Materials Conference*, Seattle, 16–19 April, 2001.
16. Udwadia FE, von Bremen H, Kumar R, Hosseini M. Time delayed control of structures. *Earthquake Engineering and Structural Dynamics* 2002; **32**:495–535.

17. Udwadia FE, Hosseini M, Chen Y-H. Robust control of uncertain system with time varying delays in input. *Proceedings of the American Control Conference*, New Mexico, 4–6 June, 1997.
18. Kobori T, Koshika N, Yamada Y, Ikeda Y. Seismic-response-controlled structure with active mass driver system, Part 1: design. *Earthquake Engineering and Structural Dynamics* 1991; **20**:133–149.
19. Koike Y, Murata T, Tanida K, Mutaguchi M, Kobori T, Ishii K, Takenaka Y, Arita T. Development of v-shaped hybrid mass damper and its application to high-rise buildings. *Proceedings of the 1st World Conference on Structural Control*, FA2-3-FA2-12, 1994.
20. Alfors LV. *Complex Analysis*. McGraw Hill: New York, 1979.